Humid periods in southern Arabia - windows of opportunity for modern human dispersal

Table of Contents

1. Supplementary Figures

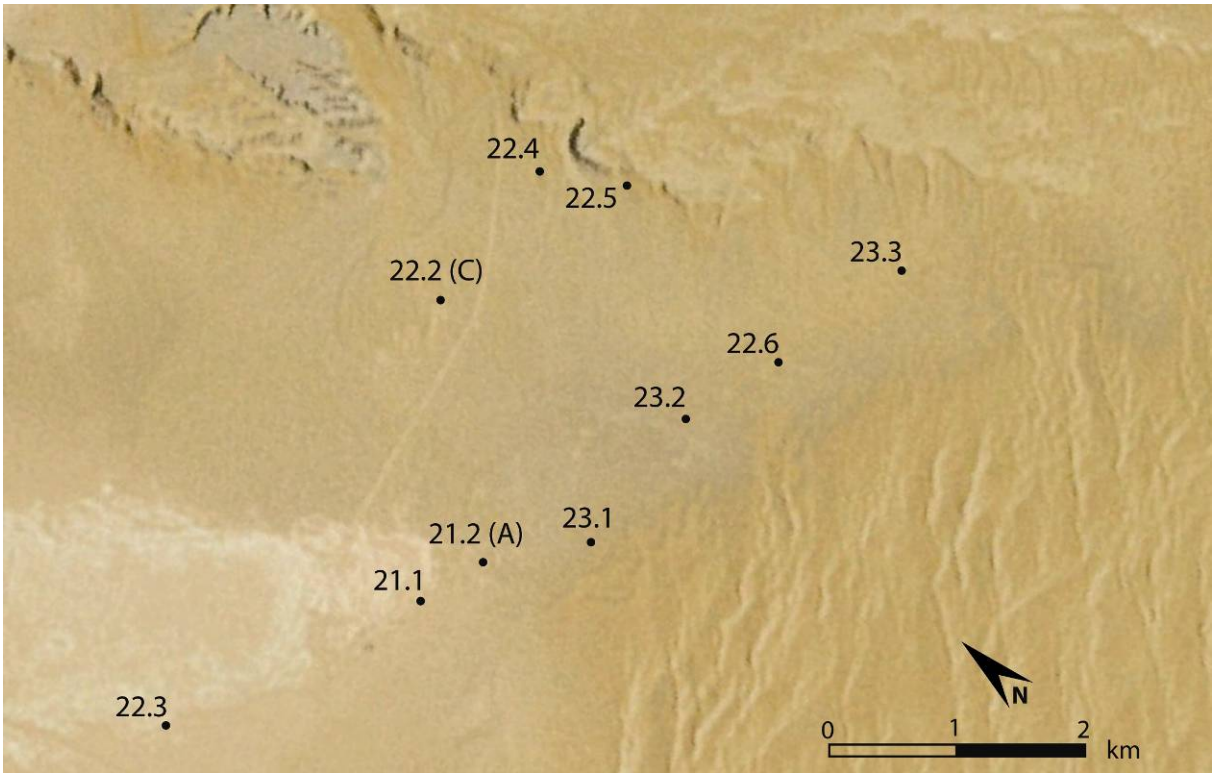

Supplementary Figure DR1. The Mundafan paleolake basin with the study sites (section numbers) and the Tuwayq escarpment in the north-east on a GoogleEarth™ image 2010.

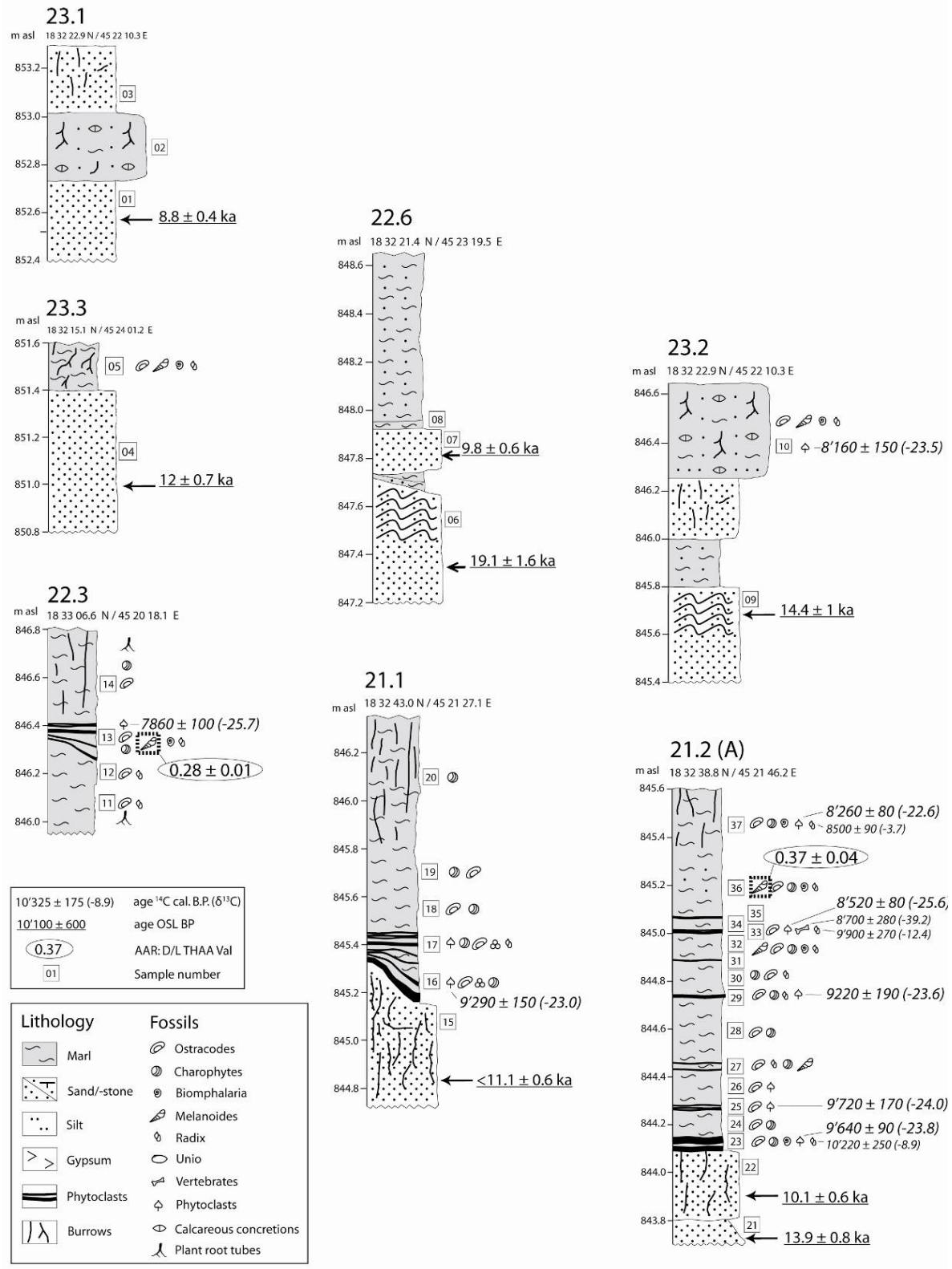

Supplementary Figure DR2. Holocene sections at Mundafan.

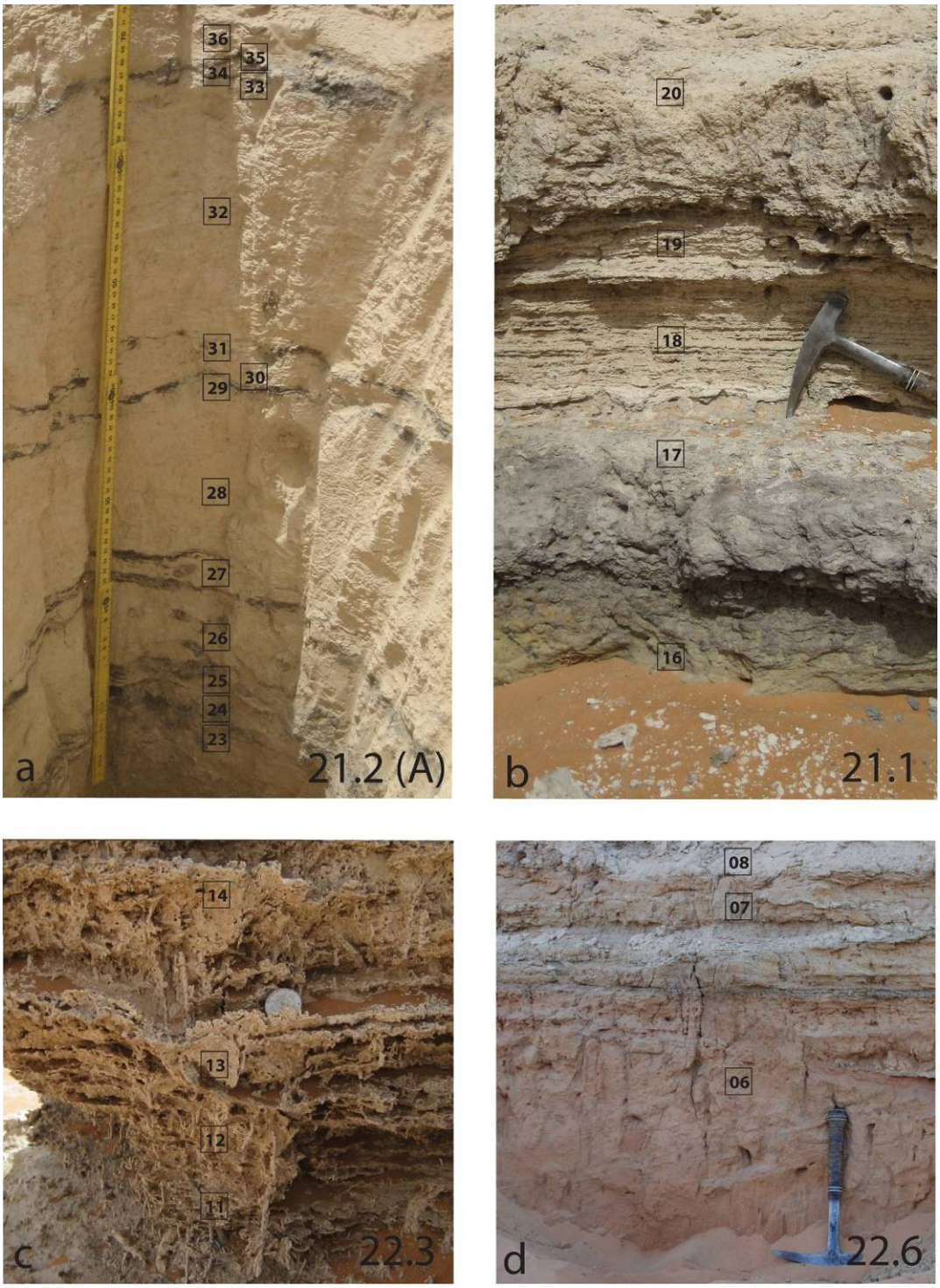

Supplementary Figure DR3. a, Section 21.2 (Sample 26-36), **b,** Section 21.1, **c,** Section 22.3, Plant root tubes and lamination. **d,** Section 22.6: Cross-bedded aeolian sand 06 below lacustrine sequence.

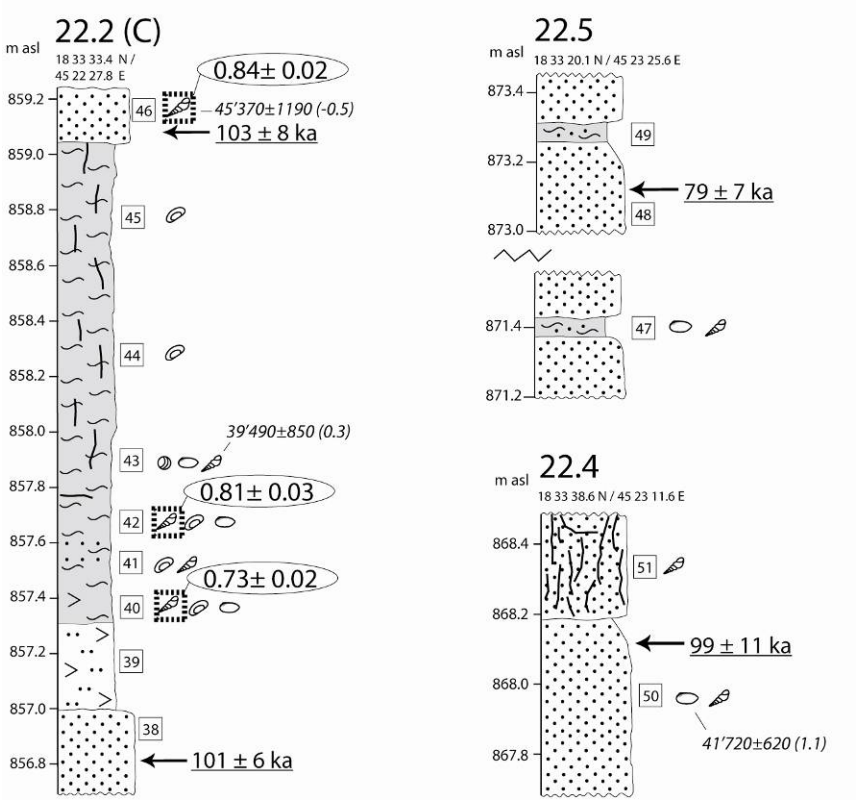

Supplementary Figure DR4. Sections at Mundafan (legend in Fig. DR2)

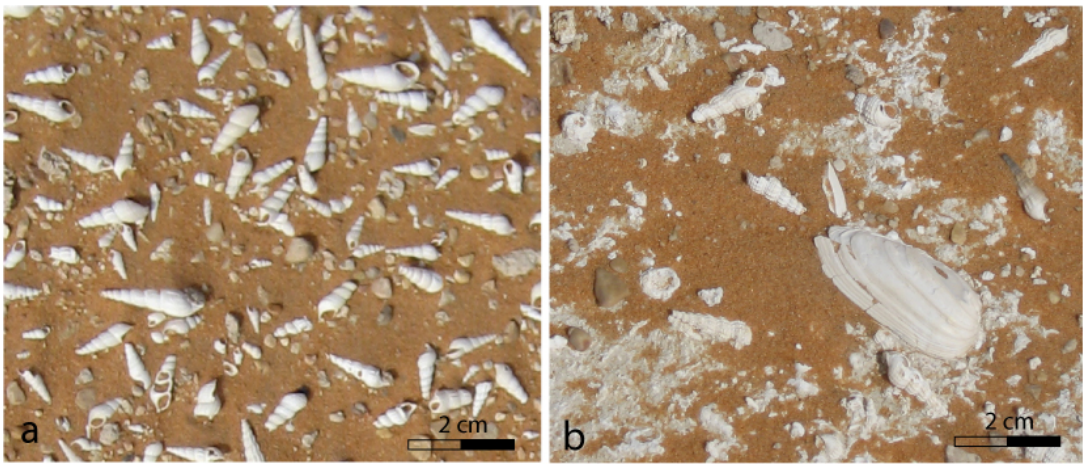

Supplementary Figure DR5. Section 22.2 (Sample 43). **a,** *Melanoides tuberculata*, **b,** *Unio* sp. and *Melanoides tuberculata*

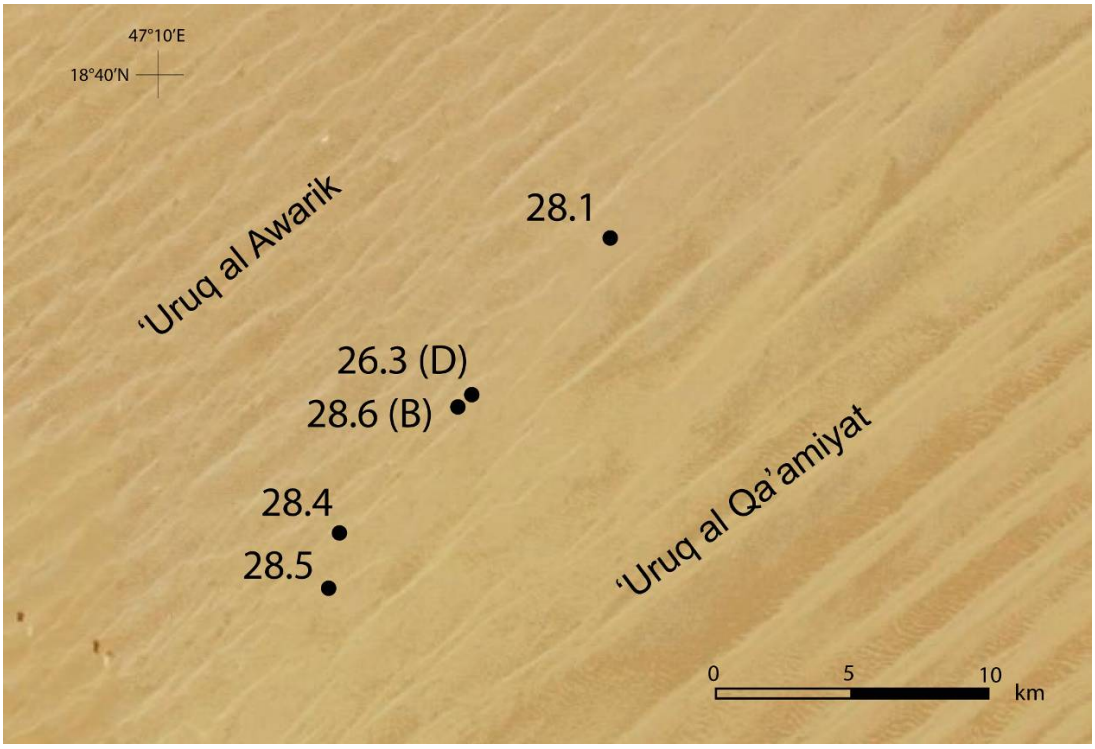

Supplementary Figure DR6. Sites (section numbers) in the Khujaymah study area, NASA World Wind image.

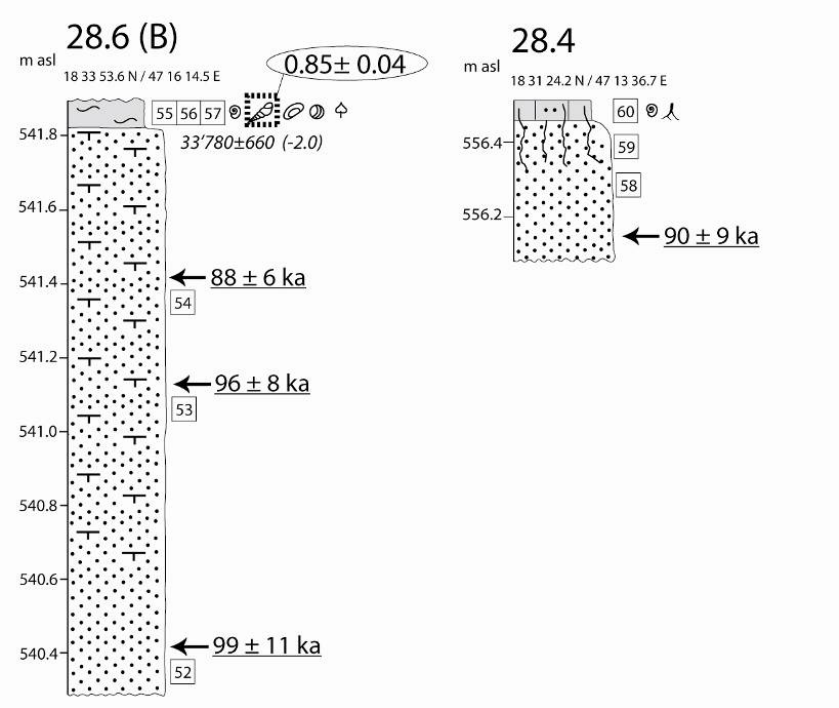

Supplementary Figure DR7. Sections at Khujaymah (legend in Fig. DR2)

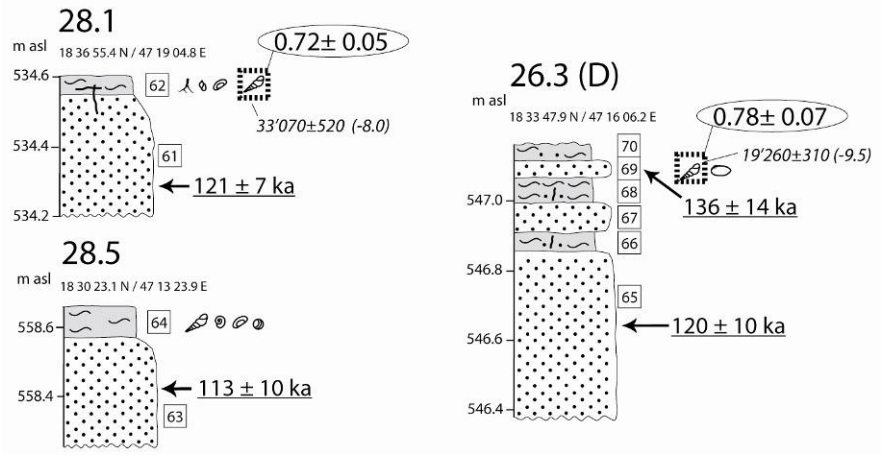

Supplementary Figure DR8. Sections at Khujaymah (legend in Fig. DR2)

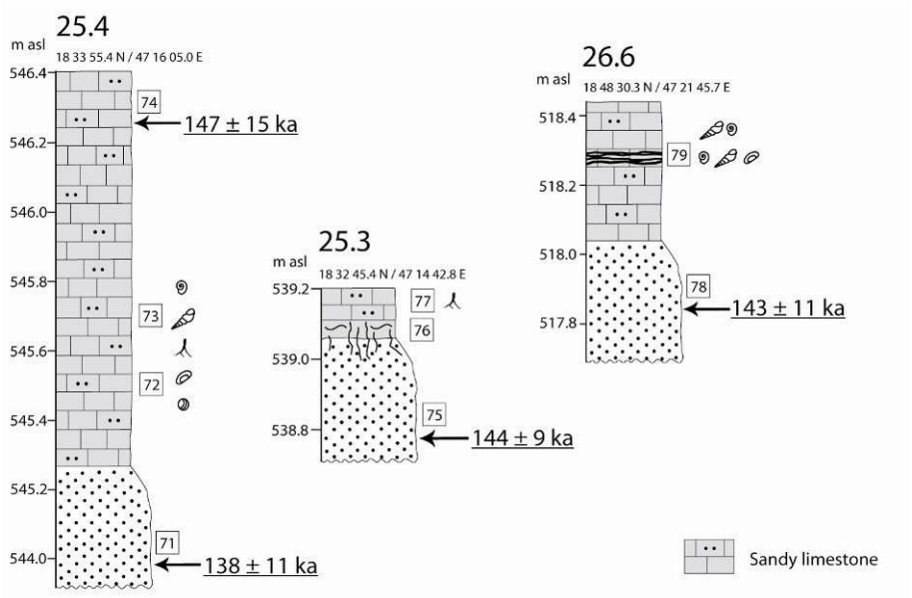

Supplementary Figure DR9. Sections at Khujaymah (legend in Fig. DR2)

Supplementary Figure DR10. Section 26.6

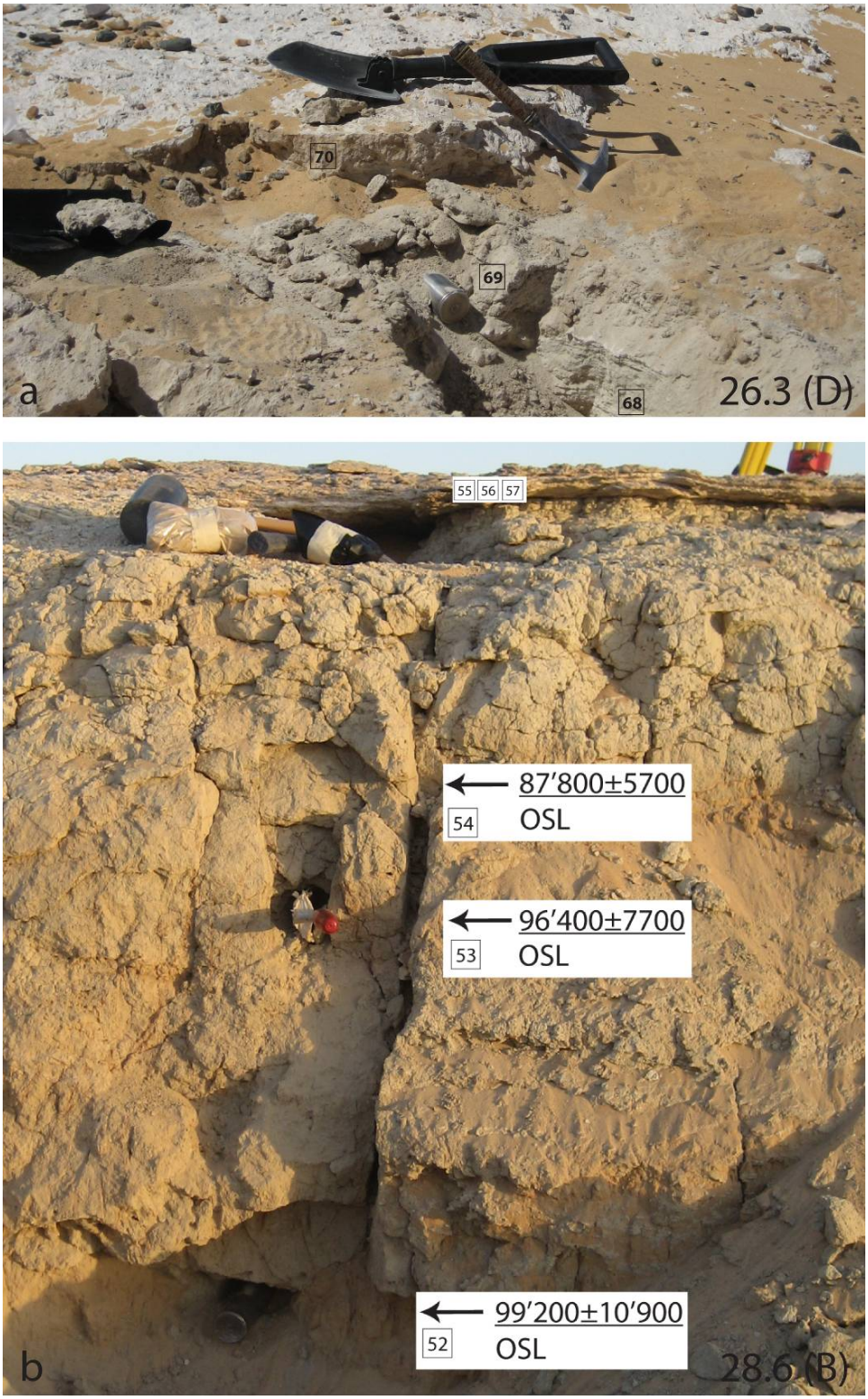

Supplementary Figure DR11. a, Section 26.3 (article Fig. 2 D), **b,** Section 28.6 (article Fig. 2 B)

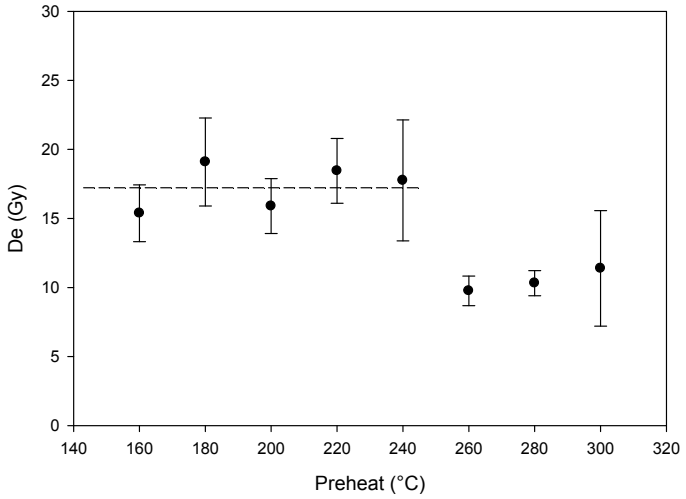

Supplementary Figure DR12. Preheat plateau test for sample 06 from section 22.6/1 (Supplementary Fig. DR2). Preheat and test dose preheat were at the same temperature and for 10 s each. Each data point it the average of 6 aliquots (2 mm).

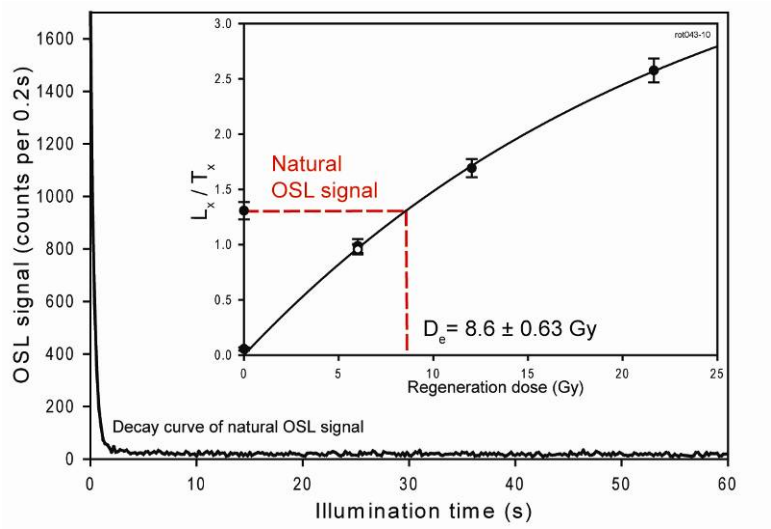

Supplementary Figure DR13. Decay curve of natural OSL (L_N) as a function of illumination time. The inset shows the growth curve of an individual aliquot, showing L_x/T_x as a function of regeneration doses. This sample (22 from section 21.2) was dated to 10.1 ± 0.6 ka.

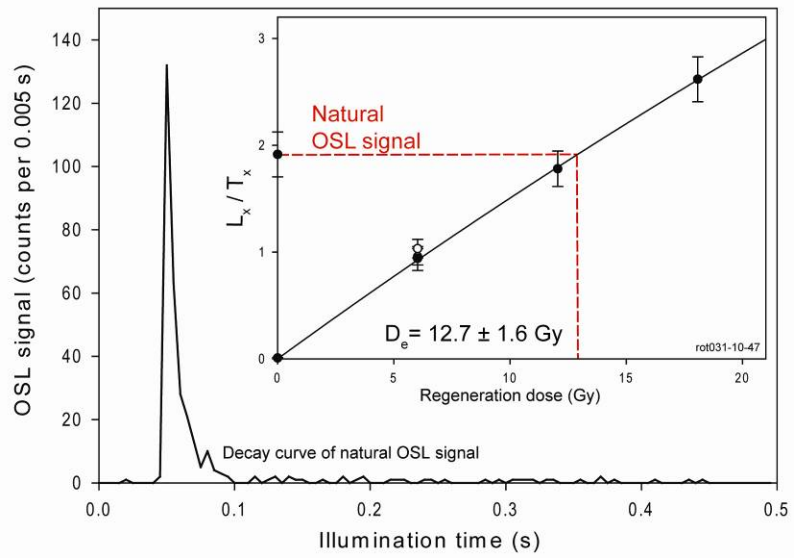

Supplementary Figure DR14. Decay curve of natural OSL (L_N) of a single grain as a function of illumination time. The inset shows the growth curve of an individual aliquot, showing L_x/T_x as a function of regeneration doses. This sample (7 from section 22.3; Supplementary Table DR4) was dated to 9.8 ± 0.5 ka.

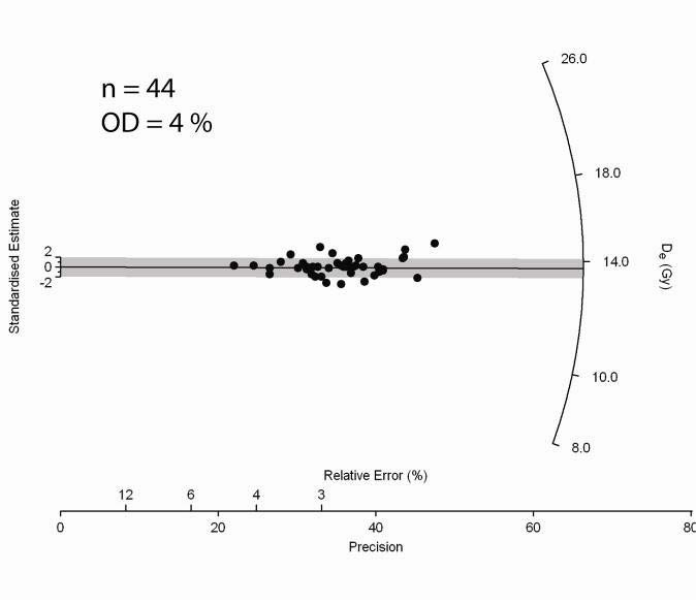

Supplementary Figure DR15. Radial plot of dose recovery test (sample 06 from section 22.6). The recovery ratio is 1.02± 0.02. Preheat and test dose preheat were 210 °C for 10s.

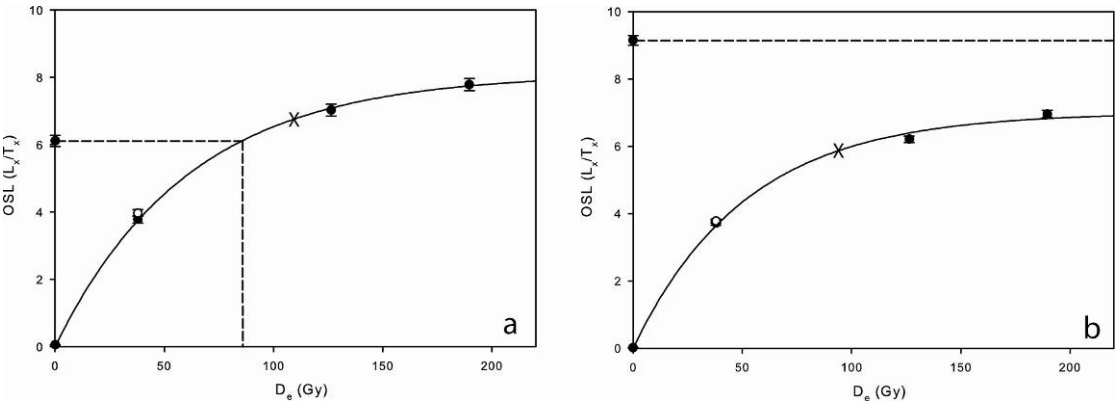

Supplementary Figure DR16. OSL dose response curves from sample 46 (section 22.2) obtained using 2 mm aliquots. The $2D_0$ values of the single saturating exponential are marked with a cross at 115 Gy (**a**) and 94 Gy (**b**). The dashed line shows the value of the natural L_n/T_n ratio. The open circle is a repeated measurement.

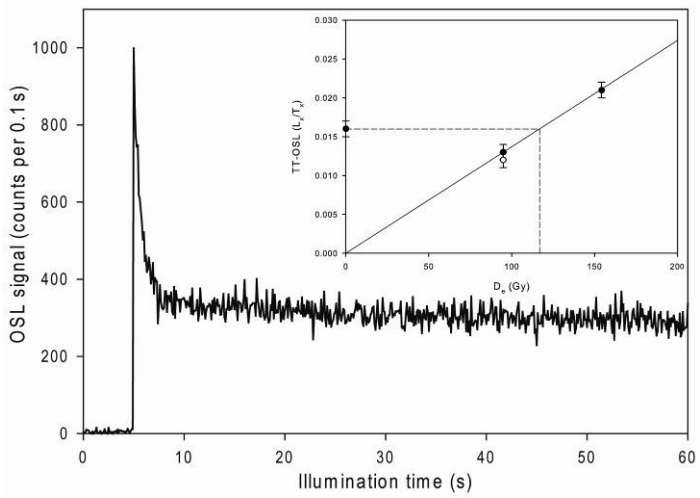

Supplementary Figure DR17. TT-OSL decay curve and TT-OSL dose response curve in the inset, both from sample 71 (section 25.4). Dose response points are linearly fitted and forced through the origin. The natural L_n/T_n ratio projected onto the curve results in a D_e of 118±10 Gy. The recycling ratio is 0.92±0.1.

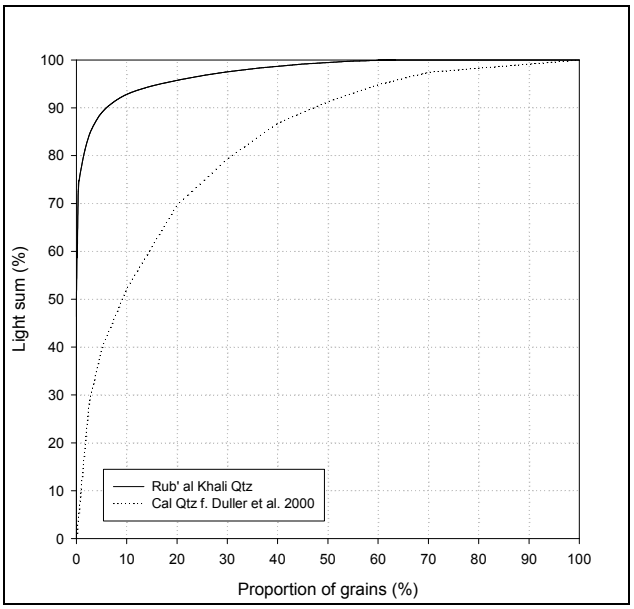

Supplementary Figure DR18. Cumulative light-sum curve from a total of 300 single grains from sample 46 compared to "calibration quartz" (Duller et al., 2000) showing that only 3 % of the grains contribute 85 % to the total light sum.

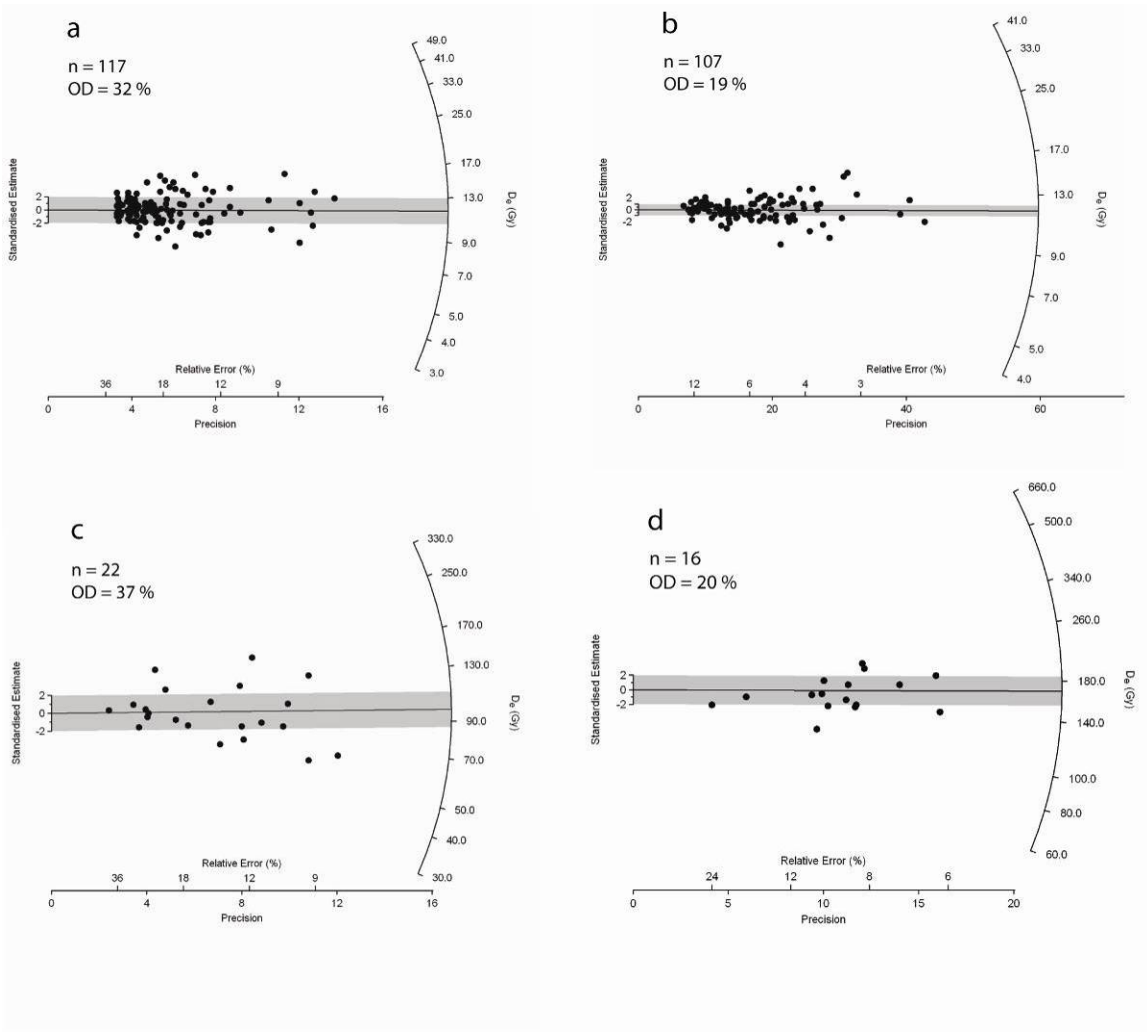

Supplementary Figure DR19. Radial plots for D_e distribution analysis. The equivalent dose for a grain is read by drawing a line from the origin of the y-axis ('Standardized Estimate') through the data point of interest, until the line intersects the radial axis (log scale) on the right-hand side. The measurement error on this equivalent dose is obtained by extending a line vertically to intersect the x-axis. The latter has two scales: the relative standard error and its reciprocal ('Precision'). **a,** Single grain D_e estimate obtained from 117 grains of quartz from a young sample (sample 6 section 22.6). **b,** 2 mm aliquot (ca. 80 grains per aliquot) D_e estimate obtained from 107 aliquots of the same young sample. **c,** Single grain D_e estimate obtained from 22 individual grains of quartz from a Pleistocene sample (sample 69 section 26.3). **d,** 6 mm aliquot (ca. 600 grains per aliquot) TT-OSL D_e estimate obtained from 16 aliquots of a Pleistocene sample (sample 54 section 28.6).

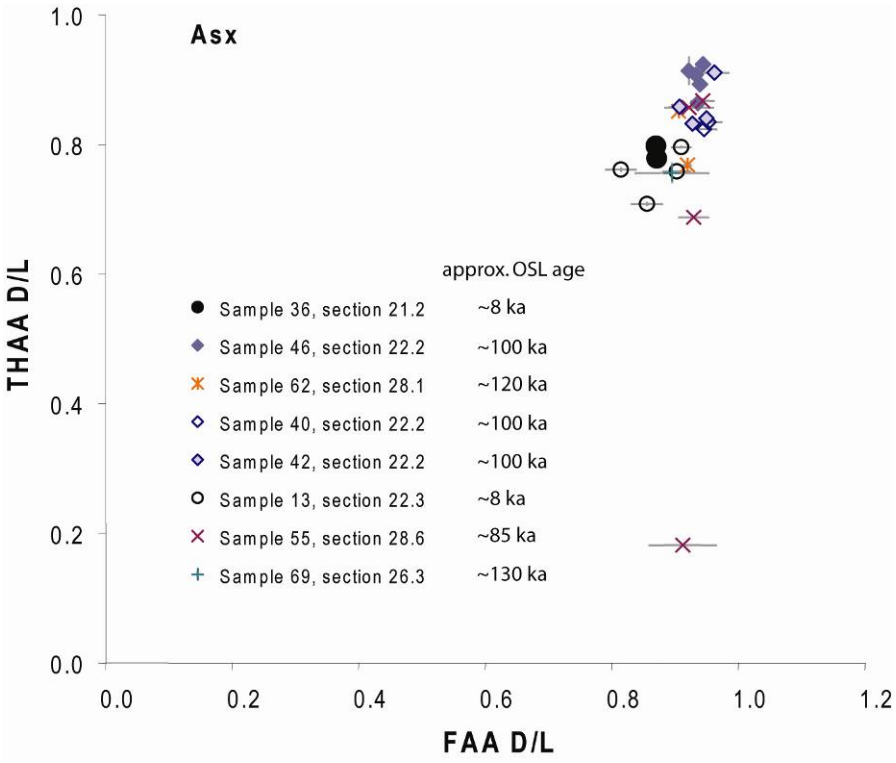

Supplementary Figure DR20. D/L THAA vs D/L FAA for Asx in *Melanoides tuberculata* shell from Mundafan.

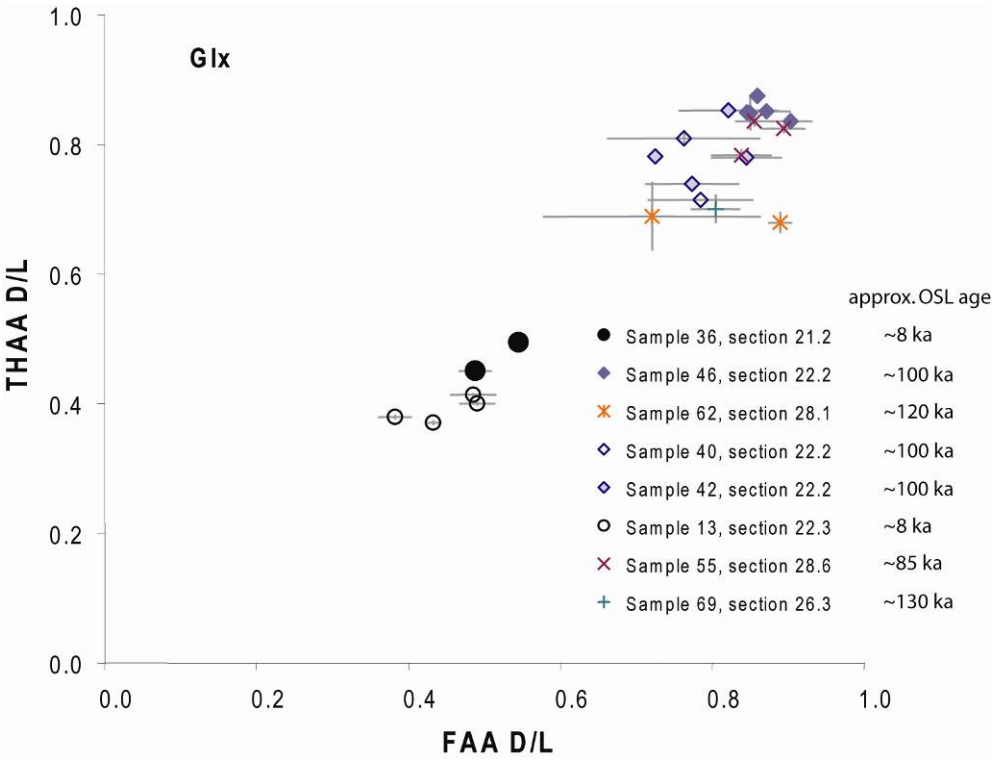

Supplementary Figure DR21. D/L THAA vs D/L FAA for Glx in *Melanoides tuberculata* shell from Mundafan and Khujaymah.

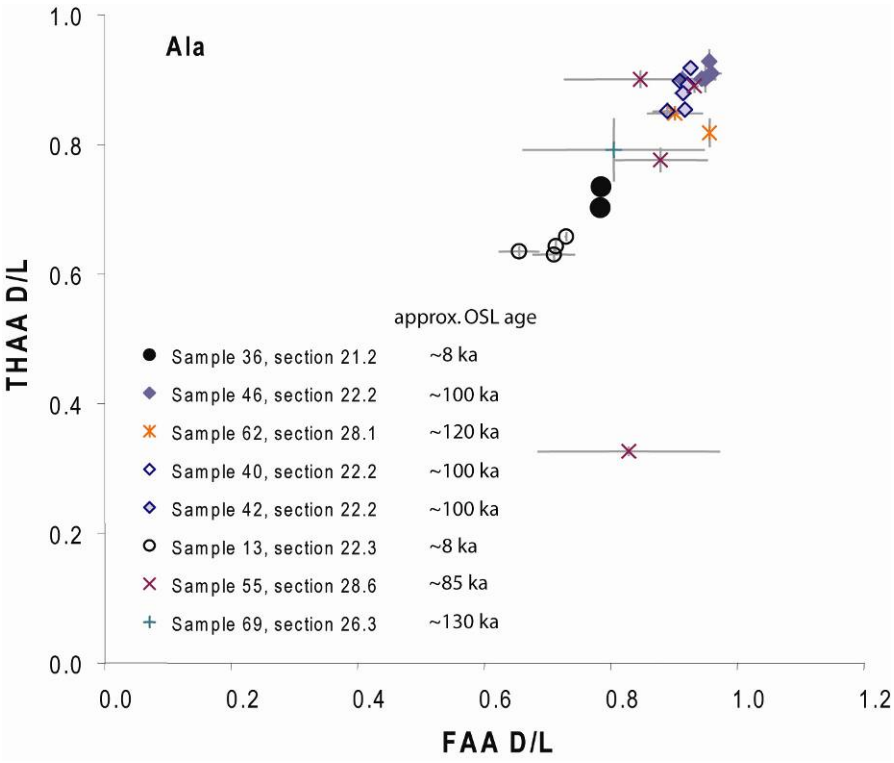

Supplementary Figure DR22. D/L THAA vs D/L FAA for Ala in *Melanoides tuberculata* shell from Mundafan and Khujaymah.

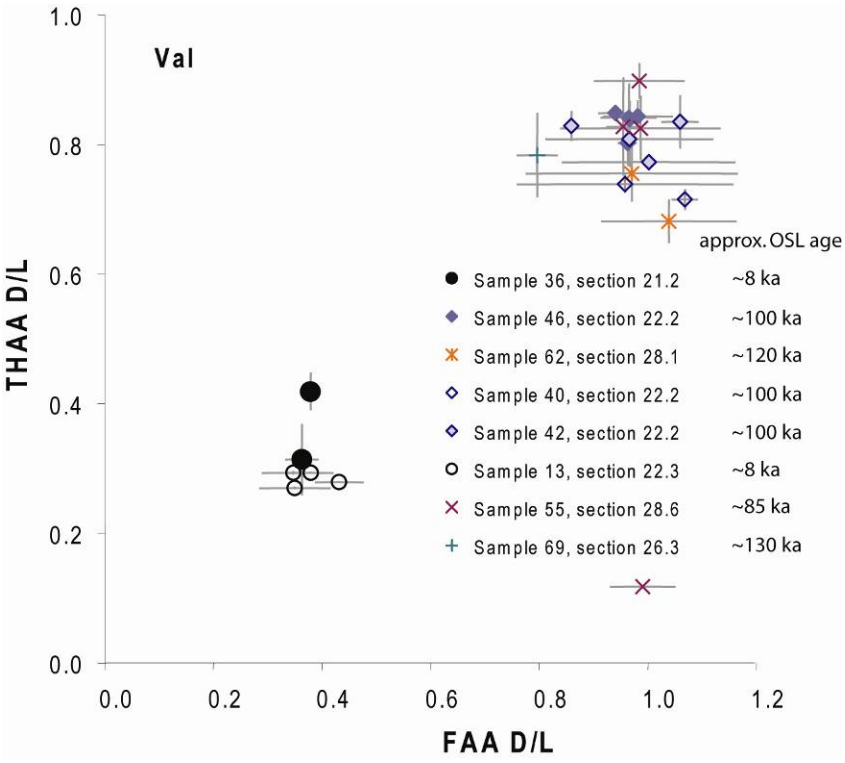

Supplementary Figure DR23. D/L THAA vs D/L FAA for Val in *Melanoides tuberculata* shell from Mundafan and Khujaymah.

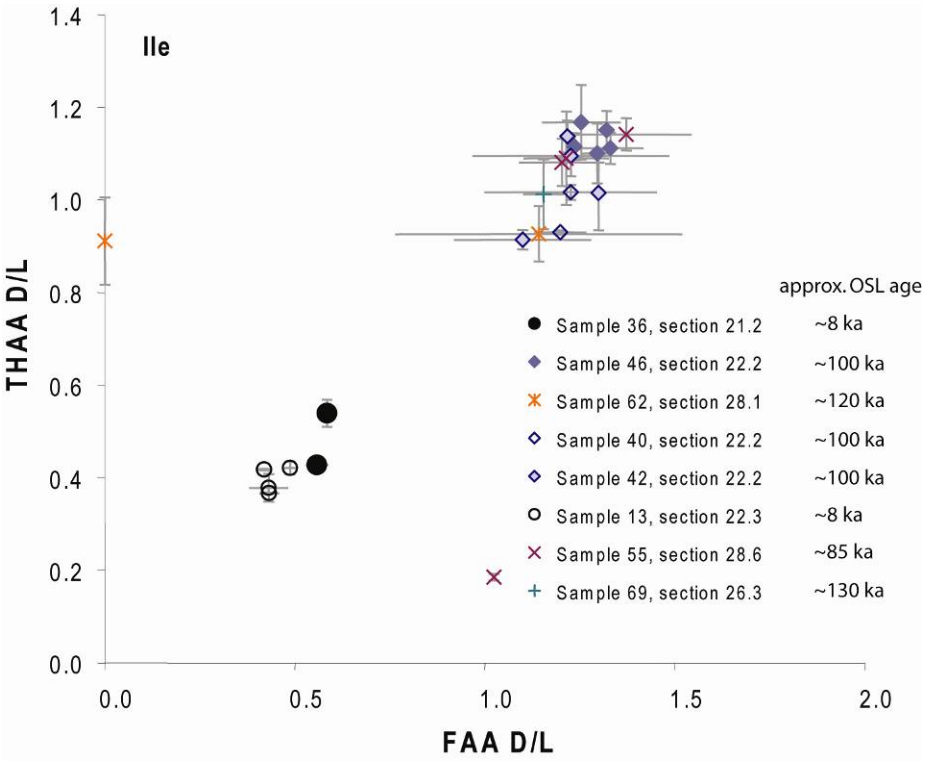

Supplementary Figure DR24. D/L THAA vs D/L FAA for L-isoleucine / D-alloisoleucine (A/I) in *Melanoides tuberculata* shell from Mundafan and Khujaymah.

2. Supplementary Methods

OSL Dating Method

Optically stimulated luminescence (OSL) dating is a method to determine burial ages of sediments. Energy supplied by naturally occurring ionizing radiation in the sediment increases the number of trapped electrons in the crystal lattice of certain mineral grains (e.g. quartz). Sunlight exposure releases light-sensitive trapped electrons. As a consequence, the intensity of the OSL signal is a measure of the radiation dose absorbed by the sediment grains since they were last exposed to daylight. For purposes of dating, the OSL signal is measured and the dose producing an equivalent signal is determined. The equivalent dose divided by the dose rate of the surrounding sediment gives the OSL age of a sample (Huntley et al., 1985).

Common problems when sampling paleolake deposits are limited sediment thickness, low quartz content and sometimes vertical inhomogeneities. The spatial and temporal (water table changes, bioturbation) homogeneity is important as it affects the dose rate, and a homogenous dose rate is generally an assumption for age estimations. As a consequence, our sampling strategy mainly relied on sampling homogenous sand beneath the lake deposits for a maximum age, combined with further samples within and/or above the lake deposits to narrow the age range of deposition. We collected samples by forcing a steel tube into a freshly cleaned exposure. The material from the tubes was then carefully discharged into opaque plastic bags for transport to the lab. Dose rate samples were collected with a small shovel from the same holes. Block samples of lithified lake deposits were wrapped with two layers of black opaque foil. Documentation of outcrops included a detailed stratigraphic sketch (Supplementary Fig. DR2-9).

All samples were opened in the laboratory under the appropriate lighting conditions (dim red/orange illumination). In the case of block samples the outer surface was removed carefully using a diamond saw with water cooling. All dating was carried out on quartz grains. The samples were treated with HCl and H_2O_2 to remove carbonates and organic matter before the grain size 200-250 µm was isolated. A two-step heavy-liquid separation using LST Fastfloat (2.70 and 2.58 g cm^{-3}) was applied and the quartz fraction was subsequently etched in HF (40%) for 60 min to reduce remaining feldspars and the outer part of the quartz grains influenced by alpha irradiation during burial. After washing with HCl to dissolve fluorides, the samples were re-sieved at 150 µm to remove remaining feldspar grains. The coarse-grained quartz was then mounted on steel discs using silicone spray or placed in special single grain discs.

The **dose rate** represents the rate of ionizing radiation to which the samples were exposed during burial and is mostly derived from the radioactive decay of ^{238}U, ^{235}U, ^{232}Th (plus their daughter products) and ^{40}K, with lesser contributions from cosmic rays. Radioactive elements (K, Th, U; Supplementary Table DR4) were measured by high-resolution gamma spectrometry

by S. Szidat, Department of Chemistry and Biochemistry, University of Bern (Preusser and Kasper, 2001). These measurements imply some evidence for radioactive disequilibrium in the Uranium decay chain for some of the samples and these have been additionally measured using Instrumental Neutron Activation Analysis (INAA) by J. Kučera, Nuclear Physics Institute Řež, Czech Republic. U-238 from INAA compared to Ra-226 from Gamma spectrometry (Supplementary Table DR4) shows limited U-238 deficiency with a negligible effect on the Pleistocene ages. For example, the age of sample 38 with extreme scenario using the values determined U-238 or Ra-226 differs not more than 3 %. Dose rates were calculated assuming average water content between 1% and 3% during burial. The contribution of cosmic rays to the total dose rate was calculated using present day depth considering full uncertainties due to actual position below surface (Prescott and Hutton, 1994). Total dose rates and resulting OSL ages are summarized in Supplementary Table DR4.

Two of the samples are rather problematic with regard to dose rate determination, as these have been taken from near surface layers. Although problematic, these samples are important as they directly date the lake deposits. Sample 74 (section 25.4) is an almost pure carbonate with little aeolian sand content. This sample shows a deficit of the mother isotope U in the decay chain and extreme low K and Th concentrations. As the layer is highly porous it appears that rain water may have reduced the concentration of radioactive elements after deposition. As a consequence, the resulting age is regarded as maximum estimate. The second problematic sample 69 (section 26.3) is from a thin aeolian sand layer bracketed by lake marls. Unfortunately, we could not measure the gamma radiation field on site, which leaves some uncertainties with regard to homogeneity. Additionally, this sample also shows low K and Th values and therefore we also regard this age as a maximum estimate.

Luminescence measurements were made in a Risø TL/OSL-DA-20 reader with blue diodes (470 ± 30 nm; ~41 mW cm^{-2}) and with a calibrated 40 mCi $^{90}Sr/^{90}Y$ beta source delivering ~0.13 Gy s^{-1} to the grains. Luminescence signals were measured with an EMI 9635Q photomultiplier tube through a 7.5 mm Hoya U340 filter. For optical stimulation of single sand-sized grains (SG) a laser attachment was used with a beam from a 10 mW Nd:YVO_4 diode-pumped green laser (532 nm) focused down to a 10 μm diameter spot with a power density of ~50 W/cm^2 (Bøtter-Jensen et al., 2000).

Early saturation of the OSL signals with $2D_0$ values between 90 - 150 Gy made it necessary to use two different protocols. Equivalent doses (D_e) were either determined with a standard SAR protocol for OSL (Murray and Wintle, 2000) or a SAR protocol for thermally transferred OSL (TT-OSL, Porat et al., 2009).

For the **Holocene samples** the single aliquot regenerative dose (SAR) protocol (Supplementary Table DR1 and DR2) of Murray and Wintle (2000) was applied to the samples

initially characterized using preheat plateau (Supplementary Fig. DR12) and dose recovery tests (Supplementary Fig. DR19).

For multi grain D_e determination a preheat of 220°C for 10 s was used and also applied to the test dose. For single grain D_e determination the conditions were the same except for the much shorter illumination of 0.5 s due to the high power density of the laser. The test dose (D_t) size was always 6 Gy. The dose response curve was constructed by plotting L_x/T_x versus dose, where L_x is the OSL signal from the regenerative dose and T_x is the response to the test dose. For multi grain the initial 0.4 s OSL signal minus a background estimated from the 50-60 s integral was used for OSL dose determinations while the much shorter intervals for single grains were 0.05-0.07 s for the signal minus a background from 0.4-0.5 s. Supplementary Figure DR13 and DR14 show representative decay and dose response curves. Aliquots were rejected if the recycling ratio was outside the range 1.0 ± 0.2 or the OSL IR depletion ratio (Duller et al., 2003) was less than 0.8. The recuperation threshold was 5 %. All heating was ramped at 5°C s^{-1}. Data analysis included a measurement error of 1 % for single aliquots and of 2.5 % for single grains. The total light sum figure (Supplementary Figure DR18) from a typical sample (48) shows that only 3 % of the grains contribute 85 % of the total light sum. We crossed-checked different aliquot sizes using single grains as well as 2 mm and 6 mm (spray mask size) multiple grain approaches (Supplementary Table DR4). The number of grains per aliquot is ~80 (2 mm) and ~600 (6 mm). The most intensively investigated samples (6 and 7) show almost identical results for the different approaches. For consistency, all ages related to the Holocene deposits shown in the figures are those determined for 2 mm aliquots (see: 4. Supplementary Discussion).

Most of the **Pleistocene samples** were out of range for the OSL SAR protocol of Murray and Wintle (2000) due to early signal saturation (Supplementary Fig. DR15). In order to date dune sands with greater expected doses, a previously published (Supplementary Table DR3, Porat et al. (2009)), single-aliquot regenerative-dose protocol (SAR) for TT-OSL was applied. A test dose of 10 Gy was used. The initial 0.4 s TT-OSL signal minus a background estimated from the 0.4-10.4 s integral, as suggested by Ballarini et al. (2007), was used for TT-OSL dose determinations (Supplementary figure DR17). For all measurements the aliquot size was 6 mm. Dose dependent dose recovery tests and recycling ratios met the standard performance criteria (Porat et al., 2009) and dose response curves demonstrated the potential to extend the dose range to beyond 600 Gy. Multiple aliquot additive dose (MAAD) TT-OSL protocols were used to test for sensitivity changes in the SAR TT-OSL protocol up to doses of 1200 Gy. A strong dose dependent deviation of the SAR TT-OSL relative to the MAAD TT-OSL dose response is observed. Comparison of the TT-OSL and OSL sensitivity data obtained from the MAAD and SAR data sets show a lack of proportionality between TT-OSL and OSL for the SAR data which will result in a problem when SAR dose response curves are constructed using many regeneration points with doses above 300 Gy. As a consequence for the samples under consideration the SAR TT-OSL protocol of Porat et al. (2009) can only be used when the

expected doses are below 300 Gy (Supplementary Fig. DR16). A detailed description of the TT-OSL testing results is given in Rosenberg et al. (2011).

AAR Dating Method

A technique of amino acid analysis has been developed for geochronological purposes (Penkman et al., 2008), combining a Reverse-Phase High Pressure Liquid Chromatography method of analysis (Kaufman and Manley, 1998) with the isolation of an "intra-crystalline" fraction of amino acids by bleach treatment (Sykes et al., 1995). This combination of techniques results in the analysis of D/L values of multiple amino acids from the chemically-protected protein within the biomineral; enabling both decreased sample sizes and increased reliability of the analysis. Amino acid analyses were undertaken on *Melanoides tuberculata* shells from Mundafan and Khujaymah. This involved isolating the intra-crystalline protein fraction of the gastropod *Melanoides tuberculata*, which is a novel species for amino acid studies. The rate of racemization is governed by a variety of factors, but the intra-crystalline amino acid fraction appears to operate as a closed system (Penkman et al., 2008; Penkman et al., 2007). Environmental factors in the intra-crystalline fraction of a particular species (e.g. water content, concentration of cations, pH) are constant and therefore the extent of racemization is a function of time and temperature. Over a small geographical area, such as that represented in this study, it can be assumed that the integrated temperature histories are effectively the same. Any differences in the extent of decomposition of protein within the sample are therefore age-dependent. The pattern of protein degradation with time is slightly different for each species and biomineral. Amino acid racemization is governed by the original protein sequence and conformation. Whilst developing the research into closed-system protein degradation it became clear that the reaction rates were species-specific, even in the intra-crystalline fraction. This necessitates the comparison of amino acid data only within a single species (Penkman et al., 2007). As *Melanoides tuberculata* has not been characterized for amino acid geochronology before, this study provides the first data as to its usefulness.

Amino acid racemization (AAR) analyses were undertaken on *Melanoides tuberculata* shells from 8 samples:

2 subsamples from sample 36, section 21.2 (Supplementary Fig. DR2), Neaar 5774, 5807, ~**8 ka**
2 subsamples from sample 40, section 22.2 (Supplementary Fig. DR4), NEaar 6003-6004, ~**100 ka**
4 subsamples from sample 42, section 22.2 (Supplementary Fig. DR4), NEaar 6005-6008, ~**100 ka**
5 subsamples from sample 46, section 22.2 (Supplementary Fig. DR4), NEaar 5775, 5808-5811, ~**100 ka**
4 subsamples from sample 13, section 22.3 (Supplementary Fig. DR2), NEaar 6009-6012, ~**8 ka**
2 subsamples from sample 69, section 26.3 (Supplementary Fig. DR8), NEaar 6017-6018, ~**130 ka**
2 subsamples from sample 62, section 28.1 (Supplementary Fig. DR8), NEaar 5776. 5812, ~**120 ka**
4 subsamples from sample 55, section 28.6 (Supplementary Fig. DR7), NEaar 6013-6016, ~**85 ka**

All samples were prepared using the procedures of (Penkman et al., 2008) to isolate the intra-crystalline protein by bleaching. Two subsamples were then taken from each shell; one fraction was directly dematerialized and the free amino acids analyzed (referred to as the 'Free' amino acids, FAA, F), and the second was treated to release the peptide-bound amino acids, thus yielding the 'total' amino acid concentration, referred to as the 'Total Hydrolysable amino acid fraction' (THAA, H*). During preparative hydrolysis both asparagine and glutamine undergo rapid irreversible deamination to aspartic acid and glutamic acid respectively. It is therefore not possible to distinguish between the acidic amino acids and their derivatives and they are reported together as Asx and Glx.

Carbon Isotope $\delta^{13}C_{org}$

Carbon isotope composition (Supplementary Table DR7) were determined using a ThermoFisher Flash-EA 1112 coupled with a Conflo IV interface to a ThermoFisher Delta V plus isotope ratio mass spectrometer (IRMS). Samples were combusted in the presence of O_2 in an oxidation column at 1030°C. Combustion gases were passed through a reduction column (650°C), and produced CO_2 gases transferred to the IRMS via an open split for on-line isotope measurements. Isotope ratios are reported in the conventional δ-notation with respect to V-PDB (Vienna Pee Dee Belemnite) standards. The methods were calibrated with NBS22 ($\delta^{13}C$ =-30.03‰) and IAEA CH-6 ($\delta^{13}C$ =-10.46‰) for carbon. Reproducibility of the measurements is better than 0.2‰.

3. Supplementary Tables

Supplementary Table DR1. OSL SAR protocol (Murray and Wintle, 2000) as used for 2 mm and 6 mm aliquots of Holocene age. For the natural sample, x = 0, D_0 = 0 Gy and the subscript n is used (L_n, T_n).

Step	Procedure
1	Dose, D_x
2	Preheat 1 at 220°C for 10 s
3	Blue stimulation at 125°C for 60 s; $\boldsymbol{L_X}$
4	Test dose, D_t = 6 Gy
5	Preheat 2 at 220°C for 10 s
6	Blue stimulation at 125°C for 60 s; $\boldsymbol{T_X}$
	Return to 1

Supplementary Table DR2. OSL SAR protocol (Murray and Wintle, 2000) as used for single grains of Holocene age. For the natural sample, x = 0, D_0 = 0 Gy and the subscript n is used (L_n, T_n).

Step	Procedure
1	Dose, D_x
2	Preheat 1 at 220°C for 10 s
3	Green laser stimulation at 125°C for 0.5 s; $\boldsymbol{L_X}$
4	Test dose, D_t = 6 Gy
5	Preheat 2 at 220°C for 10 s
6	Green laser stimulation at 125°C for 0.5 s; $\boldsymbol{T_X}$
	Return to 1

Supplementary Table DR3. Simplified TT-OSL SAR protocol as suggested by Porat et al. (2009). For the natural sample, x = 0, D_0 = 0 Gy and the subscript n is used (L_n, T_n).

Step	Procedure
1	Dose, D_x
2	Preheat at 200°C for 10 s
3	Blue stimulation at 125°C for 300 s
4	Transfer preheat at 260°C for 10 s
5	Blue stimulation at 125°C for 100 s; $\boldsymbol{L_X}$
6	Test dose, D_t
7	Preheat at 220°C for 10 s
8	Blue stimulation at 125°C for 100 s; $\boldsymbol{T_X}$
9	Heat at 300°C for 100 s
	Return to 1

Supplementary Table DR4. OSL and TT-OSL results. The grain size was always 200-250 µm and the water content 2±1 %. Doserates were calculated from high resolution Gamma spectrometry results. The highlighted data sets are the ones of the ages used.

						Activities (Bq kg^{-1})											
Nr	Section	Region	Depth (m)	Altitude (masl)	Cosmic-dose rate (mGy/ka)	K	Th	U-238 from 186 keV and Ra-226	U-238 from INAA	Ra-226	Doserate (Gy/ka)	De (Gy)	n	OD	Age (ka)	Aliquot size (mm)	Protocol
1	**23.1**	**Mund.**	**0.9**	**860**	**196**	**271.0 ± 5.7**	**8.0 ± 0.4**	**5.0 ± 3.8**		**7.2 ± 0.2**	**1.31 ± 0.06**	**11.51 ± 0.27**	**52**	**16**	**8.8 ± 0.4**	**2**	**OSL**
1	23.1	Mund.	0.9	860	196	271.0 ± 5.7	8.0 ± 0.4	5.0 ± 3.8		7.2 ± 0.2	1.31 ± 0.06	11.28 ± 0.97	7	18	8.6 ± 0.8	SG	OSL
4	**23.3**	**Mund.**	**0.6**	**860**	**203**	**207.7 ± 4.5**	**4.3 ± 0.2**	**9.2 ± 1.7**		**4.2 ± 0.1**	**1.00 ± 0.05**	**12.05 ± 0.41**	**28**	**17**	**12.0 ± 0.7**	**2**	**OSL**
6	**22.6**	**Mund.**	**1.3**	**860**	**184**	**98.0 ± 2.2**	**3.0 ± 1.1**	**3.2 ± 1.2**		**3.7 ± 0.2**	**0.62 ± 0.05**	**11.88 ± 0.24**	**107**	**19**	**19.1 ± 1.6**	**2**	**OSL**
6	22.6	Mund.	1.3	860	184	98.0 ± 2.2	3.0 ± 1.1	3.2 ± 1.2		3.7 ± 0.2	0.62 ± 0.05	11.73 ± 0.40	117	32	18.9 ± 1.7	SG	OSL
6	22.6	Mund.	1.3	860	184	98.0 ± 2.2	3.0 ± 1.1	3.2 ± 1.2		3.7 ± 0.2	0.62 ± 0.05	12.21 ± 0.45	23	17	19.6 ± 1.8	6	OSL
7	**22.6**	**Mund.**	**0.9**	**860**	**195**	**248.5 ± 5.2**	**6.4 ± 0.2**	**9.6 ± 1.9**		**6.6 ± 0.1**	**1.20 ± 0.05**	**11.72 ± 0.38**	**46**	**21**	**9.8 ± 0.5**	**2**	**OSL**
7	22.6	Mund.	0.9	860	195	248.5 ± 5.2	6.4 ± 0.2	9.6 ± 1.9		6.6 ± 0.1	1.20 ± 0.05	12.05 ± 0.52	86	30	10.0 ± 0.6	SG	OSL
7	22.6	Mund.	0.9	860	195	248.5 ± 5.2	6.4 ± 0.2	9.6 ± 1.9		6.6 ± 0.1	1.20 ± 0.05	14.09 ± 0.31	38	13	11.7 ± 0.5	6	OSL
9	**23.2**	**Mund.**	**1.0**	**860**	**192**	**207.9 ± 4.4**	**5.4 ± 0.1**	**7.6 ± 2.7**		**5.2 ± 0.2**	**1.03 ± 0.04**	**14.81 ± 0.71**	**28**	**25**	**14.4 ± 0.9**	**2**	**OSL**
9	23.2	Mund.	1.0	860	192	207.9 ± 4.4	5.4 ± 0.1	7.6 ± 2.7		5.2 ± 0.2	1.03 ± 0.04	16.77 ± 1.02	10	9	16.3 ± 1.2	SG	OSL
15	**21.1**	**Mund.**	**1.4**	**860**	**182**	**221.4 ± 4.6**	**6.0 ± 0.2**	**19.0 ± 2.6**	**27.1 ± 0.4**	**8.5 ± 0.1**	**1.13 ± 0.05**	**12.52 ± 0.40**	**47**	**15**	**<11.1 ± 0.6**	**2**	**OSL**
15	21.1	Mund.	1.4	860	182	221.4 ± 4.6	6.0 ± 0.2	19.0 ± 2.6	27.1 ± 0.4	8.5 ± 0.1	1.13 ± 0.05	12.03 ± 1.08	8	23	<10.6 ± 1.0	SG	OSL
21	**21.2**	**Mund.**	**1.8**	**860**	**172**	**172.2 ± 3.7**	**5.9 ± 0.3**	**39.9 ± 8.8**		**6.8 ± 0.2**	**0.94 ± 0.04**	**13.10 ± 0.42**	**53**	**22**	**<13.9 ± 0.8**	**2**	**OSL**
21	21.2	Mund.	1.8	860	172	172.2 ± 3.7	5.9 ± 0.3	39.9 ± 8.8		6.8 ± 0.2	0.94 ± 0.04	14.33 ± 0.52	22	16	<15.3 ± 0.9	6	OSL
22	**21.2**	**Mund.**	**1.6**	**860**	**177**	**172.4 ± 3.8**	**5.2 ± 0.3**	**21.4 ± 2.5**	**22.5 ± 0.4**	**6.1 ± 0.1**	**0.95 ± 0.04**	**9.51 ± 0.24**	**92**	**23**	**<10.1 ± 0.5**	**2**	**OSL**
22	21.2	Mund.	1.6	860	177	172.4 ± 3.8	5.2 ± 0.3	21.4 ± 2.5	22.5 ± 0.4	6.1 ± 0.1	0.95 ± 0.04	9.73 ± 0.19	52	14	<10.3 ± 0.5	6	OSL
38	**22.2**	**Mund.**	**2.5**	**860**	**157**	**433.8 ± 9.0**	**20.5 ± 0.1**	**10.6 ± 4.4**	**20.9 ± 0.4**	**16.2 ± 0.3**	**1.98 ± 0.05**	**201.05 ± 10.66**	**15**	**19**	**101 ± 6**	**6**	**TT-OSL**
38	22.2	Mund.	2.5	860	157	433.8 ± 9.0	20.5 ± 0.1	10.6 ± 4.4	20.9 ± 0.4	16.2 ± 0.3	1.98 ± 0.05	165.65 ± 11.87	17	18	>83 ± 7	SG	OSL
38	22.2	Mund.	2.5	860	157	433.8 ± 9.0	20.5 ± 0.1	10.6 ± 4.4	20.9 ± 0.4	16.2 ± 0.3	1.98 ± 0.05	130.70 ± 9.52	21	30	>65 ± 5	2	OSL
38	22.2	Mund.	2.5	860	157	433.8 ± 9.0	20.5 ± 0.1	10.6 ± 4.4	20.9 ± 0.4	16.2 ± 0.3	1.98 ± 0.05	141.30 ± 6.77	24	23	>71 ± 4	6	OSL
46	**22.2**	**Mund.**	**0.3**	**860**	**212**	**182.3 ± 4.0**	**5.9 ± 0.4**	**6.4 ± 3.2**	**11.9 ± 0.3**	**10.3 ± 0.1**	**0.97 ± 0.05**	**109.30 ± 6.76**	**12**	**18**	**103 ± 8**	**6**	**TT-OSL**
46	22.2	Mund.	0.3	860	212	182.3 ± 4.0	5.9 ± 0.4	6.4 ± 3.2	11.9 ± 0.3	10.3 ± 0.1	0.97 ± 0.05	87.60 ± 6.55	30	33	>83 ± 7	SG	OSL
46	22.2	Mund.	0.3	860	212	182.3 ± 4.0	5.9 ± 0.4	6.4 ± 3.2	11.9 ± 0.3	10.3 ± 0.1	0.97 ± 0.05	108.53 ± 7.21	23	30	>103 ± 8	2	OSL
46	22.2	Mund.	0.3	860	212	182.3 ± 4.0	5.9 ± 0.4	6.4 ± 3.2	11.9 ± 0.3	10.3 ± 0.1	0.97 ± 0.05	92.02 ± 3.28	26	18	>87 ± 5	6	OSL
48	**22.5**	**Mund.**	**0.8**	**860**	**198**	**429.8 ± 8.9**	**11.5 ± 0.6**	**12.4 ± 1.9**		**8.8 ± 0.3**	**1.79 ± 0.06**	**150.18 ± 11.40**	**11**	**24**	**79 ± 7**	**6**	**TT-OSL**
48	22.5	Mund.	0.8	860	198	429.8 ± 8.9	11.5 ± 0.6	12.4 ± 1.9		8.8 ± 0.3	1.79 ± 0.06	154.61 ± 15.00	15	29	>82 ± 9	SG	OSL
48	22.5	Mund.	0.8	860	198	429.8 ± 8.9	11.5 ± 0.6	12.4 ± 1.9		8.8 ± 0.3	1.79 ± 0.06	137.11 ± 12.54	24	43	>72 ± 7	2	OSL
48	22.5	Mund.	0.8	860	198	429.8 ± 8.9	11.5 ± 0.6	12.4 ± 1.9		8.8 ± 0.3	1.79 ± 0.06	164.08 ± 6.82	24	16	>87 ± 5	6	OSL
50	**22.4**	**Mund.**	**0.8**	**860**	**198**	**363.1 ± 7.5**	**9.1 ± 0.1**	**8.4 ± 2.0**		**9.0 ± 0.2**	**1.81 ± 0.12**	**161.63 ± 16.45**	**14**	**36**	**99 ± 11**	**6**	**TT-OSL**
50	22.4	Mund.	0.8	860	198	363.1 ± 7.5	9.1 ± 0.1	8.4 ± 2.0		9.0 ± 0.2	1.81 ± 0.12	145.52 ± 23.45	16	59	>89 ± 15	SG	OSL
50	22.4	Mund.	0.8	860	198	363.1 ± 7.5	9.1 ± 0.1	8.4 ± 2.0		9.0 ± 0.2	1.81 ± 0.12	149.43 ± 13.67	19	37	>92 ± 9	2	OSL
50	22.4	Mund.	0.8	860	198	363.1 ± 7.5	9.1 ± 0.1	8.4 ± 2.0		9.0 ± 0.2	1.81 ± 0.12	154.26 ± 5.72	18	15	>95 ± 5	6	OSL

Nr	Section	Region	Depth (m)	Altitude (masl)	Cosmic-dose rate (mGy/ka)	Activities (Bq kg^{-1}) K	Th	U-238 from 186 keV and Ra-226	U-238 from INAA	Ra-226	Doserate (Gy/ka)	De (Gy)	n	OD	Age (ka)	Aliquot size (mm)	Protocol
52	**28.6**	**Khuj.**	**1.5**	**560**	**172**	**303.7 ± 6.3**	**5.4 ± 0.1**	**5.0 ± 1.7**		**6.3 ± 0.2**	**1.23 ± 0.03**	**128.86 ± 13.32**	**8**	**18**	**99 ± 11**	**6**	**TT-OSL**
52	28.6	Khuj.	1.5	560	172	303.7 ± 6.3	5.4 ± 0.1	5.0 ± 1.7		6.3 ± 0.2	1.23 ± 0.03	63.49 ± 11.74	11	57	>49 ± 9	SG	OSL
52	28.6	Khuj.	1.5	560	172	303.7 ± 6.3	5.4 ± 0.1	5.0 ± 1.7		6.3 ± 0.2	1.23 ± 0.03	75.90 ± 7.50	25	47	>58 ± 6	2	OSL
53	**28.6**	**Khuj.**	**1.2**	**560**	**179**	**337.7 ± 7.1**	**11.3 ± 0.3**	**11.7 ± 3.2**		**15.0 ± 0.4**	**1.68 ± 0.06**	**161.51 ± 11.34**	**8**	**19**	**96 ± 8**	**6**	**TT-OSL**
53	28.6	Khuj.	1.2	560	179	337.7 ± 7.1	11.3 ± 0.3	11.7 ± 3.2		15.0 ± 0.4	1.68 ± 0.06	144.00 ± 18.00	23	39	>86 ± 11	SG	OSL
53	28.6	Khuj.	1.2	560	179	337.7 ± 7.1	11.3 ± 0.3	11.7 ± 3.2		15.0 ± 0.4	1.68 ± 0.06	137.69 ± 12.59	14	32	>82 ± 8	2	OSL
53	28.6	Khuj.	1.2	560	179	337.7 ± 7.1	11.3 ± 0.3	11.7 ± 3.2		15.0 ± 0.4	1.68 ± 0.06	131.03 ± 4.67	23	16	>78 ± 4	6	OSL
54	**28.6**	**Khuj.**	**0.5**	**560**	**197**	**406.4 ± 8.4**	**12.8 ± 0.4**	**15.7 ± 4.3**		**16.2 ± 0.2**	**1.94 ± 0.06**	**170.10 ± 9.36**	**16**	**20**	**88 ± 6**	**6**	**TT-OSL**
54	28.6	Khuj.	0.5	560	197	406.4 ± 8.4	12.8 ± 0.4	15.7 ± 4.3		16.2 ± 0.2	1.94 ± 0.06	99.92 ± 11.83	18	46	>51 ± 6	SG	OSL
54	28.6	Khuj.	0.5	560	197	406.4 ± 8.4	12.8 ± 0.4	15.7 ± 4.3		16.2 ± 0.2	1.94 ± 0.06	120.62 ± 11.22	9	10	>62 ± 6	2	OSL
58	**28.4**	**Khuj.**	**0.4**	**577**	**200**	**311.3 ± 6.5**	**5.4 ± 0.2**	**5.8 ± 2.7**		**5.2 ± 0.2**	**1.30 ± 0.01**	**119.76 ± 11.18**	**16**	**34**	**90 ± 9**	**6**	**TT-OSL**
58	28.4	Khuj.	0.4	577	200	311.3 ± 6.5	5.4 ± 0.2	5.8 ± 2.7		5.2 ± 0.2	1.30 ± 0.01	46.60 ± 7.00	13	54	>35 ± 5	2	OSL
61	**28.1**	**Khuj.**	**0.3**	**555**	**203**	**315.8 ± 6.6**	**6.5 ± 0.4**	**22.5 ± 5.6**		**15.4 ± 0.2**	**1.48 ± 0.07**	**188.88 ± 8.81**	**8**	**9**	**121 ± 7**	**6**	**TT-OSL**
61	28.1	Khuj.	0.3	555	203	315.8 ± 6.6	6.5 ± 0.4	22.5 ± 5.6		15.4 ± 0.2	1.48 ± 0.07	120.70 ± 15.50	14	46	>77 ± 10	2	OSL
63	**28.5**	**Khuj.**	**0.3**	**580**	**203**	**285.8 ± 6.0**	**6.1 ± 0.2**	**7.1 ± 1.9**		**7.7 ± 0.1**	**1.03 ± 0.04**	**147.69 ± 11.44**	**8**	**17**	**113 ± 10**	**6**	**TT-OSL**
63	28.5	Khuj.	0.3	580	203	285.8 ± 6.0	6.1 ± 0.2	7.1 ± 1.9		7.7 ± 0.1	1.03 ± 0.04	143.60 ± 4.65	13	8	>110 ± 6	2	OSL
65	**26.3**	**Khuj.**	**0.8**	**570**	**189**	**253.2 ± 5.4**	**5.5 ± 0.3**	**8.1 ± 3.0**	**7.7 ± 0.3**	**6.7 ± 0.2**	**1.12 ± 0.01**	**141.14 ± 10.01**	**8**	**15**	**120 ± 10**	**6**	**TT-OSL**
65	26.3	Khuj.	0.8	570	189	253.2 ± 5.4	5.5 ± 0.3	8.1 ± 3.0	7.7 ± 0.3	6.7 ± 0.2	1.12 ± 0.01	107.74 ± 6.33	17	23	>92 ± 7	2	OSL
65	26.3	Khuj.	0.8	570	189	253.2 ± 5.4	5.5 ± 0.3	8.1 ± 3.0	7.7 ± 0.3	6.7 ± 0.2	1.12 ± 0.01	113.50 ± 4.82	18	17	**>97** ± 6	6	OSL
69	**26.3**	**Khuj.**	**0.1**	**570**	**210**	**143.7 ± 3.1**	**2.5 ± 0.2**	**3.9 ± 2.4**	**5.5 ± 0.2**	**5.9 ± 0.1**	**0.73 ± 0.01**	**108.07 ± 9.83**	**8**	**20**	**136 ± 14**	**6**	**TT-OSL**
69	26.3	Khuj.	0.1	570	210	143.7 ± 3.1	2.5 ± 0.2	3.9 ± 2.4	5.5 ± 0.2	5.9 ± 0.1	0.73 ± 0.01	97.65 ± 8.55	22	34	>123 ± 12	SG	OSL
71	**25.4**	**Khuj.**	**1.3**	**570**	**177**	**275.1 ± 5.8**	**5.3 ± 0.2**	**6.1 ± 2.6**	**10.2 ± 0.3**	**9.2 ± 0.3**	**1.3 ± 0.05**	**175.64 ± 11.68**	**16**	**24**	**138 ± 11**	**6**	**TT-OSL**
71	25.4	Khuj.	1.3	570	177	275.1 ± 5.8	5.3 ± 0.2	6.1 ± 2.6	10.2 ± 0.3	9.2 ± 0.3	1.3 ± 0.05	136.83 ± 21.03	12	44	>108 ± 17	SG	OSL
74	**25.4**	**Khuj.**	**0.2**	**570**	**206**	**22.7 ± 0.8**	**0.7 ± 0.2**	**11.0 ± 4.9**	**18.0 ± 0.3**	**25.0 ± 0.3**	**0.8 ± 0.04**	**111.15 ± 9.46**	**12**	**32**	**147 ± 15**	**6**	**TT-OSL**
74	25.4	Khuj.	0.2	570	206	22.7 ± 0.8	0.7 ± 0.2	11.0 ± 4.9	18.0 ± 0.3	25.0 ± 0.3	0.8 ± 0.04	93.90 ± 3.17	10	9	>124 ± 8	2	OSL
74	25.4	Khuj.	0.2	570	206	22.7 ± 0.8	0.7 ± 0.2	11.0 ± 4.9	18.0 ± 0.3	25.0 ± 0.3	0.8 ± 0.04	103.27 ± 3.56	20	15	>140 ± 8	6	OSL
75	**25.3**	**Khuj.**	**0.5**	**560**	**197**	**263.9 ± 5.5**	**4.5 ± 0.2**	**4.9 ± 2.0**		**6.0 ± 0.2**	**1.2 ± 0.05**	**170.91 ± 8.32**	**7**	**26**	**144 ± 9**	**6**	**TT-OSL**
75	25.3	Khuj.	0.5	560	197	263.9 ± 5.5	4.5 ± 0.2	4.9 ± 2.0		6.0 ± 0.2	1.2 ± 0.05	155.50 ± 27.30	15	66	>131 ± 24	SG	OSL
75	25.3	Khuj.	0.5	560	197	263.9 ± 5.5	4.5 ± 0.2	4.9 ± 2.0		6.0 ± 0.2	1.2 ± 0.05	157.40 ± 16.20	10	30	>133 ± 15	2	OSL
78	**26.6**	**Khuj.**	**0.7**	**540**	**191**	**275.7 ± 5.7**	**4.3 ± 1.2**	**6.5 ± 1.7**		**7.7 ± 0.1**	**1.2 ± 0.06**	**177.96 ± 9.79**	**8**	**7**	**143 ± 11**	**6**	**TT-OSL**
78	26.6	Khuj.	0.7	540	191	275.7 ± 5.7	4.3 ± 1.2	6.5 ± 1.7		7.7 ± 0.1	1.2 ± 0.06	157.84 ± 12.40	10	22	>127 ± 12	2	OSL

Supplementary Table DR5. Amino acid data for *Melanoides tuberculata* from Mundafan and Khujaymah. Error terms represent one standard deviation about the mean. Each sample was bleached, with the free amino acid fraction signified by 'FAA' and the total hydrolysable fraction by 'THAA'.

		FAA								THAA							
		Asx D/L		Glx D/L		Ala D/L		Val D/L		Asx D/L		Glx D/L		Ala D/L		Val D/L	
Sample	Neaar ı	x	σ	x	σ	x	σ	x	σ	x	σ	x	σ	x	σ	x	σ
Sample 13	6009	0.910	0.016	0.485	0.030	0.729	0.002	0.347	0.058	0.796	0.002	0.414	0.003	0.658	0.007	0.293	0.003
Sample 13	6010	0.903	0.023	0.490	0.024	0.713	0.001	0.350	0.066	0.758	0.001	0.400	0.003	0.643	0.012	0.270	0.002
Sample 13	6011	0.814	0.025	0.382	0.022	0.655	0.032	0.380	0.042	0.761	0.003	0.380	0.004	0.635	0.008	0.293	0.002
Sample 13	6012	0.856	0.026	0.433	0.011	0.710	0.034	0.432	0.045	0.708	0.003	0.371	0.004	0.630	0.012	0.279	0.001
Sample 13		**0.871**	**0.044**	**0.448**	**0.051**	**0.702**	**0.032**	**0.377**	**0.039**	**0.756**	**0.036**	**0.391**	**0.020**	**0.642**	**0.012**	**0.284**	**0.011**
Sample 36	5774	0.870	0.008	0.545	0.012	0.785	0.010	0.379	0.006	0.798	0.000	0.495	0.009	0.735	0.004	0.419	0.029
Sample 36	5807	0.871	0.007	0.488	0.022	0.783	0.004	0.363	0.031	0.778	0.001	0.451	0.007	0.702	0.007	0.314	0.055
Sample 36		**0.870**	**0.001**	**0.516**	**0.040**	**0.784**	**0.001**	**0.371**	**0.011**	**0.788**	**0.014**	**0.473**	**0.031**	**0.718**	**0.023**	**0.366**	**0.074**
Sample 40	6003	0.953	0.022	0.763	0.101	0.909	0.013	1.068	0.024	0.835	0.001	0.809	0.009	0.898	0.003	0.715	0.016
Sample 40	6004	0.946	0.021	0.785	0.069	0.889	0.024	0.958	0.200	0.824	0.001	0.714	0.002	0.852	0.013	0.739	0.014
Sample 40		**0.949**	**0.022**	**0.774**	**0.085**	**0.899**	**0.018**	**1.013**	**0.112**	**0.829**	**0.008**	**0.762**	**0.067**	**0.875**	**0.033**	**0.727**	**0.017**
Sample 42	6005	0.962	0.024	0.822	0.066	0.926	0.005	1.060	0.034	0.911	0.002	0.853	0.002	0.918	0.004	0.835	0.041
Sample 42	6006	0.949		0.725		0.922		0.859		0.840	0.003	0.782	0.001	0.892	0.004	0.829	0.023
Sample 42	6007	0.907	0.017	0.774	0.062	0.917	0.007	0.966	0.155	0.858	0.005	0.739	0.006	0.854	0.006	0.809	0.044
Sample 42	6008	0.927	0.013	0.845	0.047	0.914	0.014	1.002	0.160	0.832	0.002	0.780	0.006	0.879	0.001	0.773	0.013
Sample 42		**0.937**	**0.024**	**0.791**	**0.053**	**0.920**	**0.005**	**0.972**	**0.084**	**0.860**	**0.035**	**0.788**	**0.047**	**0.886**	**0.027**	**0.811**	**0.028**
Sample 46	5775	0.936	0.005	0.903	0.029	0.943	0.024	0.965	0.052	0.864	0.009	0.836	0.010	0.901	0.001	0.841	0.053
Sample 46	5808	0.933	0.008	0.872	0.032	0.913	0.000	0.967	0.014	0.908	0.010	0.851	0.012	0.900	0.014	0.839	0.028
Sample 46	5809	0.922	0.003	0.846	0.002	0.959	0.017	0.940	0.032	0.914	0.022	0.849	0.009	0.910	0.006	0.849	0.012
Sample 46	5810	0.944	0.011	0.859	0.010	0.955	0.001	0.982	0.064	0.924	0.012	0.875	0.009	0.928	0.019	0.844	0.024
Sample 46	5811	0.939	0.004	0.850	0.000	0.949	0.000	0.963	0.018	0.893	0.006	0.848	0.027	0.902	0.021	0.802	0.035
Sample 46		**0.935**	**0.008**	**0.866**	**0.023**	**0.944**	**0.018**	**0.963**	**0.015**	**0.900**	**0.023**	**0.852**	**0.014**	**0.908**	**0.012**	**0.835**	**0.019**
Sample 55	6013	0.943	0.019	0.894	0.029	0.932	0.007	0.987	0.148	0.868	0.004	0.825	0.008	0.891	0.011	0.825	0.050
Sample 55	6014	0.912	0.054	0.836	0.005	0.828	0.144	0.991	0.061	*0.1817	*0.000	*0.138	*0.001	*0.326	*0.007	*0.117	*0.001
Sample 55	6015	0.922	0.039	0.855	0.025	0.846	0.121	0.984	0.083	0.857	0.000	0.836	0.008	0.901	0.014	0.898	0.027
Sample 55	6016	0.929	0.025	0.839	0.040	0.879	0.075	0.955	0.031	0.688	0.002	0.783	0.009	0.776	0.019	0.828	0.076
Sample 55		**0.927**	**0.013**	**0.856**	**0.027**	**0.871**	**0.045**	**0.979**	**0.016**	**0.804**	**0.101**	**0.815**	**0.028**	**0.856**	**0.069**	**0.850**	**0.041**
Sample 62	5776	0.920	0.007	0.890	0.016	0.901	0.044	1.039	0.125	0.768	0.001	0.680	0.016	0.848	0.004	0.682	0.034
Sample 62	5812	0.906	0.006	0.721	0.144	0.956	0.000	0.971	0.196	0.851	0.009	0.689	0.053	0.818	0.022	0.755	0.043
Sample 62		**0.913**	**0.010**	**0.805**	**0.119**	**0.929**	**0.038**	**1.005**	**0.048**	**0.810**	**0.059**	**0.684**	**0.007**	**0.833**	**0.021**	**0.718**	**0.052**
Sample 69	6017	0.895	0.059	0.804	0.033	0.804	0.144	0.797	0.038	0.756	0.016	0.701	0.022	0.792	0.049	0.784	0.065
Sample 69	6018	0.902	0.052	0.798	0.002	0.801	0.167	0.855	0.007								
Sample 69		**0.898**	**0.005**	**0.801**	**0.004**	**0.803**	**0.002**	**0.826**	**0.041**	**0.756**	**0.016**	**0.701**	**0.022**	**0.792**	**0.049**	**0.784**	**0.065**

*not included in average due to contamination

Supplementary Table DR6. Radiocarbon dating results. Calibration was done with OxCal 4.10 using the IntCal09 curve (Bronk Ramsey, 2009). Preparation and measurement procedure are described in Hajdas et al. (2004). Samples with the comment "leach+" were subject to additional HCl leaching.

Sec	Nr	Lab Nr.	Material	DeltaC13 (‰)	C14 age BP	Cal (2σ) age (OxCal 4.10) BP	Comment
21.2	37	ETH-38514	Phytoclasts	-22.6 ± 1.1	7420 ± 35	8260 ± 80	
21.2	37	ETH-36454	Shell, Lymnea	-3.7 ± 1.2	7720 ± 55	8500 ± 90	
21.2	33	ETH-36452	Bone, Vertebrate	-39.2 ± 1.1	7810 ± 70	8700 ± 280	
21.2	33	ETH-36453	Shell, Lymnea	-12.4 ± 1.2	8820 ± 65	9900 ± 270	
21.2	33	ETH-37794	Phytoclasts	-25.6 ± 1.1	7755 ± 40	8520 ± 80	
21.2	29	ETH-37793	Phytoclasts	-23.6 ± 1.1	8255 ± 45	9220 ± 190	
21.2	25	ETH-38512	Phytoclasts	-24.0 ± 1.1	8710 ± 35	9720 ± 170	
21.2	23	ETH-38511	Phytoclasts	-23.8 ± 1.1	8685 ± 35	9640 ± 90	
21.2	23	ETH-36567	Phytoclasts (raw)	-2.2 ± 1.2	9300 ± 40	10480 ± 175	
21.2	23	ETH-36451	Shell, Lymnea	-8.9 ± 1.2	9075 ± 60	10220 ± 250	
21.1	16	ETH-37792	Phytoclasts	-23.0 ± 1.1	8300 ± 45	9290 ± 150	
22.3	13	ETH-37906	Phytoclasts	-25.7 ± 1.1	7030 ± 40	7860 ± 100	
23.2	10	ETH-37907	Phytoclasts	-23.5 ± 1.4	7325 ± 50	8160 ± 150	
22.2	43	ETH-36455	Shell, Melanoides	0.3 ± 1.2	31570 ± 420	35930 ± 870	
22.2	43	ETH-36455-	Shell, Melanoides	-4.1 ± 1.2	34350 ± 320	39490 ± 850	leach+
22.2	46	ETH-36456	Shell, Melanoides	-0.5 ± 1.2	38065 ± 895	42830 ± 1350	
22.2	46	ETH-36456-	Shell, Melanoides	-1.9 ± 1.2	41785 ± 770	45370 ± 1190	leach+
22.4	50	ETH-36457	Shell, Unio	1.1 ± 1.2	34065 ± 580	39040 ± 1630	
22.4	50	ETH-36457-	Shell, Unio	-2.5 ± 1.2	36755 ± 415	41720 ± 620	leach+
28.6	55	ETH-38709	Marl, bulk	-2.0 ± 1.1	28970 ± 135	33780 ± 660	
26.3	55	ETH-38710	Shell, Unio	-9.5 ± 1.1	16230 ± 50	19260 ± 310	
28.1	62	ETH-38711	Shell, Melanoides	-8.0 ± 1.1	28685 ± 125	33070 ± 520	

Supplementary Table DR7. Carbon isotope $\delta^{13}C_{org}$ ratios

Sample (Fig. DR2)	Weight (mg)	Run	$\delta^{13}C_{org}$ VPDB (‰)
16	4.856	NC0183	-24.830
23	6.077	NC0183	-24.844
29	4.791	NC0183	-25.976
37	9.142	NC0183	-26.141
13	6.489	NC0183	-25.918
10	6.206	NC0183	-23.233

4. Supplementary Discussion

Discussion of OSL dating

Sources of scatter in D_e distributions include the variability in luminescence sensitivity and dose saturation characteristics (Roberts et al., 1999; Duller et al., 2000), incomplete bleaching (Olley et al., 1998), variations in microdosimetry (Murray and Roberts, 1997; Kalchgruber et al., 2003; Vandenberghe et al, 2003), and post-depositional mixing (Roberts et al., 1999). While incomplete bleaching and post-depositional mixing increases the spread of the distribution by skewed distributions or a mixture of different populations, variations in microdosimetry and the variability in sensitivity and saturation characteristics only generally increases the spread of the distribution. The samples from Mundafan and Khujaymah were tested for mixed populations by single grain methodology. Single grain D_e distributions (Supplementary Fig. DR19a,c) show little skewness and only a single population ruling out problems of incomplete bleaching and post-depositional mixing.
In order to describe D_e distributions quantitatively, a parameter defining the spread of the distribution was calculated. The over-dispersion parameter (OD) is defined as the spread in a population that is additional to the spread expected from the error on each individual D_e value (Galbraith et al., 1999), which is strongly influenced by differences in signal intensity. The OD of the samples under consideration (Supplementary Table DR4) is on average 20 %, ranging from 15 to 25 % for the Holocene samples (2 mm aliquots). Such broad distributions have previously been observed for dune sands from Southern Australia and have been attributed to variations in microdosimetry (Kalchgruber et al. 2003). Appling the decision process of Bailey and Arnold (2006) shows that none of the distributions from Holocene samples has a skew that indicates a mixture of populations. In order to obtain a central value that best reflects the average D_e of each sample, the central age model (Galbraith et al., 1999) was chosen for calculations.

For the Holocene deposits (Supplementary Fig. DR2), it is shown that all OSL ages for the dune sands below the lake deposits are predating the onset of lake formation, as given by radiocarbon, by not more than a few thousand years. We hence assume that the deposition of aeolian sand below the lake deposits in general usually just predates the onset of lake formation. This assumption has been applied for the Pleistocene deposits and is supported by evidence from sections 22.2 (Supplementary Fig. DR4), 26.2 (Supplementary Fig. DR8) and 25.4 (Supplementary Fig. DR9).

Discussion AAR geochronology

The DL ratios of Asx, Glx, serine (Ser), alanine (Ala) and valine (Val) provide an overall estimate of protein decomposition. These indicators of protein decomposition have been selected as their peaks are cleanly eluted with baseline

separation and they cover a wide range of rates of reaction. It is expected that with increasing age, the extent of racemization (D/L) will increase.
If the amino acids were contained within a closed system, the relationship between the FAA and the THAA fractions should be highly correlated, with non-concordance enabling the recognition of compromised samples (Preece and Penkman, 2005). The plot of FAA to THAA data from each sample can also be used as a relative timescale, with younger samples falling towards the bottom left corner of the graph and older samples falling towards the upper right corner, along the line of expected decomposition. The data from the Mundafan samples have been plotted in this way for each of the amino acids. As the site of Mundafan has experienced a different temperature history to that of previous studies of intra-crystalline protein degradation, correlation to absolute dates requires the development of an aminostratigraphic framework for this area.

Asparagine (Asx) is one of the fastest racemizing of the amino acids discussed here (due to the fact that it can racemize whilst still peptide bound). This enables good levels of resolution at younger age sites, but decreased resolution with older material. The D/L Asx data from the Holocene samples have the lowest values of the samples analyzed, as expected. However, most of the other horizons are nearing equilibrium, meaning that Asx is not particularly useful for age resolution for sites of this age. The subsamples of sample 55 are divergent – 6014bH* shows very low D/L values in the THAA fraction, falling away from the line of expected decomposition, along with high concentrations and a differing amino acid composition. This sample shows clear signs of contamination, so although the data is presented in the figures, it should not be used for age determination.

Glutamine (Glx) is one of the slower racemizing amino acids discussed here and so the low levels of racemization do help discriminate between material of the ages of this study. It is noteworthy that Glx has a slightly unusual pattern of racemization in the free form, due to the formation of a lactam. This results in difficulties in measuring Glx in the Free form, as the lactam cannot be derivitized and is therefore unavailable for analysis. The Glx D/L values from sample 13 show the lowest values (Supplementary Fig. DR23), with sample 36 yielding slightly higher D/L values, consistent with their relative radiocarbon dates within the Holocene. Again, the 6014bH* subsamples from sample 55 show that their closed system has been compromised and should be rejected. The other sites show high levels of racemization, nearing equilibrium, although sample 62 and sample 69 exhibit the lower values of the group. Sample 46, sample 51 and sample 40 show similar levels of protein breakdown, consistent with relatively rapid deposition of this sequence.

Alanine (Ala) is a hydrophobic amino acid, whose concentration is partly contributed from the decomposition of other amino acids (notably serine). Ala racemizes at an intermediate rate, so is one of the amino acids that may help distinguishing samples of the timescales under consideration. The results for Ala are

broadly similar to that seen in the other amino acids (Supplementary Fig. DR24). The alanine data supports the interpretation that sample 13 is the youngest in age, with sample 36 slightly older. The 6014bH* subsamples from sample 55 again show divergence from closed system behavior. The replication of sample 55 and sample 69 samples is not particularly good, so further samples are being run to confirm this. Sample 62 tend to show a slightly younger age, with sample 46, sample 42 and sample 40 showing tight clustering at almost equilibrium levels.

Valine (Val) has extremely low rates of racemization, and as the concentration of Val is quite low, the difficulty of measuring the D/L accurately results in higher variability. It does however still prove useful for age discrimination within material of Pleistocene age. The Val D/L in the FAA and THAA fractions again support the other amino acid data (Supplementary Fig. DR23). The Holocene samples are demonstrably younger, while the one subsample from sample 55 is compromised. Data from sample 62 is more variable, but still consistent with a younger age than sample 46, sample 42 and sample 40 (but significantly older than the Holocene samples). Again, the older samples show values nearing equilibrium; it is therefore likely that AAR dating has reached its temporal limit for this area.

Isoleucine (Ile) also has extremely low rates of racemization, and baseline separation is not very accurate using the RP-HPLC technique, so is usually separated by ion exchange chromatography. However, results are presented here as they support the data obtained from the other amino acids. Isoleucine has two chiral centers, but the important geochronological reaction is the breakdown of L-isoleucine to its diastereomer D-alloisoleucine, which is reported to equilibrate at D/L values of 1.3 (often reported as an A/I value). Again, the Holocene samples are clearly distinguishable, and the other sites are tending towards equilibrium.

The *Melanoides tuberculata* samples seem to show relatively good closed system behavior, although a higher degree of variability is seen within sample 62, and there is clear contamination in sample 55. While optical thin section analysis showed that the structure of the shells is well preserved, there were indications of epitaxial calcite growth. Our preparation isolates the intra-crystalline material within a shell, therefore we are theoretically analyzing a closed system of protein. However, if any re-crystallization has occurred, then this compromises the intra-crystalline fraction, meaning it has not been closed system for the history of the sample, and therefore cannot be used for dating. It may be that the variability is due to re-crystallization, but the relative consistency between the amino acids would argue against any significant effect. The two samples of well-constrained Holocene age: Sample 13 (~ 8000 years BP) and sample 36 (~9000 years BP) show levels of protein degradation consistent with these ages. The rest of the samples show levels of racemization nearing equilibrium, limiting their relative resolution. At what point equilibrium is achieved with these species in this tropical environment is unknown. Further study will inform on this. Using AAR, it is not possible to discriminate between the three

samples analyzed which have been excavated within a sequence (sample 46, sample 42 and sample 40).

In this study, the amino acid data has been used as a relative dating technique to present a pilot aminostratigraphy for the area in question. The conversion of relative sequences into absolute dates and accurate correlation between different areas requires further studies on the patterns of breakdown in *Melanoides tuberculata*. However, it is concluded that sample 13 and sample 36 are the youngest within the sequence, consistent with their radiocarbon ages. Very high levels of protein degradation are observed in the other samples, inconsistent with a Holocene age. Amino acid geochronology has the potential to yield useful information on the relative age of these deposits in this area, but it is vital to establish the time point where equilibration occurs to constrain these ages.

Discussion Radiocarbon Dating

For understanding the discrepancy between Pleistocene OSL and radiocarbon ages, it is important to realize that samples (mainly porous mollusk shells; e.g. *Melanoides tuberculata*) used for radiocarbon dating of pre-Holocene deposits will have strongly been affected by epitaxial calcite growth due to the interaction with water during the Holocene humid period, leading to an incorporation of younger ^{14}C. In section 22.2 (Supplementary Fig. DR4) radiocarbon ages of *Melanoides tuberculata* shells (39,490 ± 850 cal BP (sample 43) and 45,370 ± 1190 cal BP (sample 46)) are stratigraphically inverted. OSL ages of ~100 ka for aeolian deposits from above and below the same lacustrine sequence are considered to reflect the real depositional age. Additional leaching on the same samples (43, 46 and also 50) had only increased the age by 3.5 ka, 2.5 ka and 2.7 ka but was not able to remove all of the epitaxial calcite due to the porous structure of the shells. This problem has been reported on other occasions from similar environments (Fontes and Gasse, 1989). The Holocene radiocarbon ages (Supplementary Fig. DR2) on shells on the other hand show some hard water effect with the ages on shells being up to 1.4 ka older than the ages on phytoclasts.

Discussion Ostracodes

Ostracode species from Mundafan and Khujaymah are typical of fresh- to brackish, shallow water environments. Most prominent species include *Cyprideis torosa* that mainly occurs in marine brackish waters with fluctuating salinities but is also characteristic of a wide range of continental water bodies down to a water depth of 30 m (McClure, 1980; Meisch, 2000). Other species that tolerate an increase in salinity are *Cypris* sp., *Cypris bispinosa*, and *Heterocypris salina* (Meisch, 2000). Freshwater species include *Cypretta* sp., a genus usually found in warm (often subtropical), shallow, vegetated waters (Bronshtein, 1947; Smith and Delorme, 2010) and *Paracandona* sp. that prefers small water bodies with a swampy or boggy bottom

and the littoral zone of lakes (Meisch, 2000). A species that needs stable conditions and cannot survive in desiccating environments is *Darwinula stevensoni.* This species lives in aquifers and seeps (Bronshtein, 1947; Griffiths et al., 2001; Martens et al., 1997; Schwalb, 2003; Smith and Delorme, 2010) and also occurs in the littoral of lakes, rivers, bogs and springs (Dumont et al., 1986; Martens et al., 1997). Less characteristic and less abundant are *Candona* sp. and *Limnocythere* sp., both benthonic species as well as *Candonocypris* sp., a nektobenthonic species that is an indicator for running shallow waters (Pérez et al., 2010).

Each humid phase is characterized by a typical species assemblage (number of samples):

Holocene (16), *Paracandona* sp. is accompanied by *Cypris* sp., *Darwinula stevensoni*, and *Heterocypris salina*. This suggests small and shallow, permanent and possibly slightly saline environments.

~80 ka (3), *Darwinula stevensoni* is the dominant ostracode. This species is accompanied by *Paracandona* sp., *Cypris* sp., and a few specimen of *Cyprideis torosa*. This suggests significantly fresher conditions than during the Holocene and at ~100 ka with permanent water bodies.

~100 ka (5), The dominance of *Cyprideis torosa* hints at brackish waters. The presence of *Candonocypris* sp., *Darwinula stevensoni*, and *Limnocythere* sp. suggests the existence of permanent, shallow water bodies with possibly running water.

~125 ka (1), *Darwinula stevensoni* is the dominant species accompanied by *Cypris* sp. and *Paracandona* sp. This suggests significantly fresher conditions than during the Holocene and at ~100 ka with permanent water bodies.

References Supplementary Materials

Bailey, R. M., and Arnold, L. J., 2006, Statistical modelling of single grain quartz De distributions and an assessment of procedures for estimating burial dose: Quaternary Science Reviews, v. 25, no. 19-20, p. 2475-2502.

Ballarini, M., Wallinga, J., Wintle, A. G., and Bos, A. J. J., 2007, A modified SAR protocol for optical dating of individual grains from young quartz samples: Radiation Measurements, v. 42, no. 3, p. 360-369.

Bøtter-Jensen, L., Bulur, E., Duller, G. A. T., and Murray, A. S., 2000, Advances in luminescence instrument systems: Radiation Measurements, v. 32, no. 5-6, p. 523-528.

Bronk Ramsey, C., 2009, Bayesian analysis of radiocarbon dates. Radiocarbon, v. 51, p. 337-360.

Bronshtein, Z. S., 1947, Fresh-water Ostracoda Fauna of the USSR Crustaceans (Amerind Publishing for the U.S. Dept. of the Interior / N.S.F., New Delhi). [English transl., 1988.], v. 2 (1), no. i-xv, p. 1-470.

Duller, G. A. T., 2003, Distinguishing quartz and feldspar in single grain luminescence measurements: Radiation Measurements, v. 37, no. 2, p. 161-165.

Duller, G. A. T., Bøtter-Jensen, L., and Murray, A. S., 2000, Optical dating of single sand-sized grains of quartz: sources of variability: Radiation Measurements, v. 32, no. 5-6, p. 453-457.

Dumont, H. J., Maas, S., and Martens, K., 1986, Cladocera, Copepoda and Ostracoda (Crustacea) from Fresh Waters in South Yemen: Fauna of Saudi Arabia, v. 8, no. 12-19.

Fontes, J. C., and Gasse, F., 1989, On the ages of humid Holocene and Late Pleistocene phases in North Africa -- Remarks on "Late Quaternary climatic reconstruction for the Maghreb (North Africa)" by P. Rognon: Palaeogeography, Palaeoclimatology, Palaeoecology, v. 70, no. 4, p. 393-398.

Galbraith, R. F., Roberts, R. G., Laslett, G. M., Yoshida, H., and Olley, J. M., 1999, Optical dating of single and multiple grains of Quartz from Jinmium rock shelter, Northern Australia: Part I, Experimental design and statistical models: Archaeometry, v. 41, no. 2, p. 339-364.

Griffiths, H. I., Schwalb, A., and Stevens, L. R., 2001, Evironmental change in southwestern Iran: the Holocene ostracod fauna of Lake Mirabad: The Holocene, v. 11, no. 6, p. 757-764.

Hajdas, I., Bonani, G., Thut, J., Leone, G., Pfenninger, R., and Maden, C., 2004, A report on sample preparation at the ETH/PSI AMS facility in Zurich: Nuclear Instruments and Methods in Physics Research Section B: Beam Interactions with Materials and Atoms, v. 223-224, p. 267-271.

Huntley, D.J., Godrey-Smith, D.I. and Thewalt, M.L.W., 1985, Optical dating of sediments: Nature, v. 313, p. 105-107

Kalchgruber, R., Fuchs, M., Murray, A. S., and Wagner, G. A., 2003, Evaluating dose-rate distributions in natural sediments using [alpha]-Al2O3:C grains: Radiation Measurements, v. 37, no. 4-5, p. 293-297.

Kaufman, D. S., and Manley, W. F., 1998, A new procedure for determining dl amino acid ratios in fossils using reverse phase liquid chromatography: Quaternary Science Reviews, v. 17, no. 11, p. 987-1000.

Martens, K., Rossetti, G., and Fuhrmann, R., 1997, Pleistocene and Recent species of the family Darwinulidae: Hydrobiologia, v. 357, p. 99-116.

McClure, H. A., Swain, F.M., 1980, Fresh-water and Brackish-water fossils Quaternary Ostracoda from the Rub' al Khali ("Empty Quater"), Saudi Arabia: Actes du VI Colloque Africain de Micropaléontologie - Tunis 1974, Annales des Mines et de la Géologie, v. 28, p. 427-441.

Meisch, C., 2000, Freshwater Ostracoda of Western and Central Europe, Süßwasserfauna von Mitteleuropa 8/3: Heidelberg, Spektrum Akademischer Verlag, 1-522 p.

Murray, A. S., and Roberts, R. G., 1997, Determining the burial time of single grains of quartz using optically stimulated luminescence: Earth and Planetary Science Letters, v. 152, no. 1-4, p. 163-180.

Murray, A. S., and Wintle, A. G., 2000, Luminescence dating of quartz using an improved single-aliquot regenerative-dose protocol: Radiation Measurements, v. 32, no. 1, p. 57-73.

Olley, J., Caitcheon, G., and Murray, A., 1998, The distribution of apparent dose as determined by optically stimulated luminescence in small aliquots of fluvial quartz: implications for dating young sediments: Quaternary Science Reviews, v. 17, no. 11, p. 1033-1040.

Penkman, K. E. H., Kaufman, D. S., Maddy, D., and Collins, M. J., 2008, Closed-system behaviour of the intra-crystalline fraction of amino acids in mollusc shells: Quaternary Geochronology, v. 3, no. 1-2, p. 2-25.

Penkman, K. E. H., Preece, R. C., Keen, D. H., Maddy, D., Schreve, D. C., and Collins, M. J., 2007, Testing the aminostratigraphy of fluvial archives: the evidence from intra-crystalline proteins within freshwater shells: Quaternary Science Reviews, v. 26, no. 22-24, p. 2958-2969.

Pérez, L., Lorenschat, J., Bugja, R., Brenner, M., Scharf, B., and Schwalb, A., 2010, Distribution, diversity and ecology of modern freshwater ostracodes (Crustacea), and hydrochemical characteristics of Lago Petén Itzá, Guatemala: Journal of Limnology, v. 69, no. 1, p. 146-159.

Porat, N., Duller, G. A. T., Roberts, H. M., and Wintle, A. G., 2009, A simplified SAR protocol for TT-OSL: Radiation Measurements, v. 44, no. 5-6, p. 538-542.

Preece, R. C., and Penkman, K. E. H., 2005, New faunal analyses and amino acid dating of the Lower Palaeolithic site at East Farm, Barnham, Suffolk: Proceedings of the Geologists Association, v. 116, p. 363-377.

Prescott, J. R., and Hutton, J. T., 1994, Cosmic ray contributions to dose rates for luminescence and ESR dating: Large depths and long-term time variations: Radiation Measurements, v. 23, no. 2-3, p. 497-500.

Preusser, F., and Kasper, H. U., 2001, Comparison of dose rate determination using high-resolution gamma spectrometry and inductively coupled plasma - mass spectrometry: Ancient TL, v. 19, no. 1, p. 19-23.

Roberts, R. G., Galbraith, R. F., Olley, J. M., Yoshida, H., and Laslett, G. M., 1999, Optical dating of single and multiple grains of quartz from Jinmium rock shelter, Northern Australia: Part II, Results and implications: Archaeometry, v. 41, no. 2, p. 365-395.

Rosenberg, T. M., Preusser, F., and Wintle, A. G., 2011, A comparison of single and multiple aliquot TT-OSL data sets for sand-sized quartz from the Arabian Peninsula: Radiation Measurements.

Schwalb, A., 2003, Lacustrine ostracodes as stable isotope recorders of late-glacial and Holocene environmental dynamics and climate: Journal of Paleolimnology, v. 29, no. 3, p. 265-351.

Smith, A. J., and Delorme, L. D., 2010, Ostracoda, Ecology and Classification of North American Freshwater Invertebrates p. 725-771.

Sykes, B., Leiboff, A., Low-Beer, J., Tetzner, S., and Richards, M., 1995, The origins of the Polynesians: An interpretation from mitochondrial lineage analysis: Am. J. Hum. Genet., v. 57, p. 1463 - 1475.

Vandenberghe, D., Hossain, S. M., De Corte, F., and Van den haute, P., 2003, Investigations on the origin of the equivalent dose distribution in a Dutch coversand: Radiation Measurements, v. 37, no. 4-5, p. 433-439.

Wintle, A. G., and Murray, A. S., 2006, A review of quartz optically stimulated luminescence characteristics and their relevance in single-aliquot regeneration dating protocols: Radiation Measurements, v. 41, no. 4, p. 369-391.